IIETA International Information and Engineering Technology Association
Advancing the World of Information and Engineering

Journal Européen des Systèmes Automatisés
Vol. 59, No. 4, April, 2026, pp. 881-903
Journal homepage: http://iieta.org/journals/jesa

Adaptive Fuzzy Logic-Based Power Distribution Strategy for Four-Wheel-Drive Fuel Cell Electric Vehicles with Hybrid Energy Storage Systems

Mammeri Khaled*, Gasbaoui Brahim, Hamza Tedjini

Laboratory of Smart Grids, Renewable Energies (SGRE), Faculty of Technology, Department of Electrical Engineering, Tahri Mohamed University of Bechar, Bechar 08000, Algeria

Corresponding Author Email: mammeri.khaled@univ-bechar.dz

https://doi.org/10.18280/jesa.590403

Received: 31 January 2026
Revised: 2 April 2026
Accepted: 11 April 2026
Available online: 30 April 2026

Keywords:
adaptive fuzzy logic, state of charge, component lifespan, four-wheel drive, hydrogen consumption, proton exchange membrane fuel cell, transient power demand, real-time control

ABSTRACT

This paper presents an adaptive fuzzy logic-based energy management strategy (AFLC-EMS) for a four-wheel drive fuel cell electric vehicle (FCEV) with a proton exchange membrane fuel cell (PEMFC), lithium-ion battery, and supercapacitor hybrid energy storage system. The vehicle uses four synchronous reluctance motors (15 kW each, 60 kW total). The adaptive fuzzy controller dynamically distributes power among the energy sources based on battery and supercapacitor state of charge (SoC), power demand, and its rate of change. A secondary fuzzy controller enables real-time adaptation of power distribution coefficients (α_i) within bounded ranges [0.5, 1.5] and with rate limiting ($0.05\ s^{-1}$) to ensure stability. A frequency-based power splitting strategy optimizes supercapacitor use for transient demands while preserving battery longevity. Simulations under Worldwide Harmonized Light Vehicles Test Procedure (WLTP), Urban Dynamometer Driving Schedule (UDDS), and Highway Fuel Economy Test (HWFET) cycles show hydrogen consumption of 0.82 kg/100 km (0.74 for UDDS and 0.91 for HWFET), representing a 12.8% improvement over rule-based strategies and reaching 96.2% of the dynamic programming (DP) optimum. The battery SoC is maintained within 45–75%, and the fuel cell operates mainly in its high-efficiency range (50–60%). Degradation analysis indicates a 60.9% extension in fuel cell lifetime and an 18.3% reduction in battery stress. Real-time feasibility is validated with execution times below 2.34 ms. Overall, the AFLC-EMS enhances system efficiency while extending component lifespan.

1. INTRODUCTION

The global transition toward sustainable transportation has accelerated the development of zero-emission vehicles, with fuel cell electric vehicles (FCEVs) emerging as a promising solution for long-range applications [1]. Unlike battery electric vehicles, FCEVs provide rapid refueling capabilities and extended driving ranges, making them particularly suitable for commercial and heavy-duty applications [2].

Recent industrial deployments have demonstrated the viability of FCEV technology, with operational fleets in Shenzhen (China) accumulating over 8 million kilometers across 300 fuel cell buses [3], and Toyota's second-generation Mirai achieving hydrogen consumption of 0.79-0.84 kg/100km under real-world conditions [4].

Modern FCEVs typically employ hybrid energy storage systems (HESS), combining fuel cells, batteries, and supercapacitors to overcome the limitations of each technology [5]. The proton exchange membrane fuel cell (PEMFC) offers high energy density but suffers from slow dynamic response and efficiency degradation under fluctuating loads [6]. Lithium-ion batteries provide moderate power density and energy storage capability but are sensitive to high-current transients, which accelerate degradation [7].

Supercapacitors excel in handling rapid power fluctuations with high efficiency and virtually unlimited cycle life, although their energy density remains limited [8].

Field data from 50,000 km FC truck trials show that HESS configuration strongly affects cost, with three-source systems improving component longevity by 15-22% over two-source setups [9]. The energy management strategy (EMS) is essential for optimizing power distribution to enhance efficiency and reduce hydrogen consumption [10]. Existing approaches include rule-based [11], optimization-based methods such as dynamic programming (DP) [12] and MPC [13], and intelligent techniques like fuzzy logic and neural networks [14].

Recent literature (2023–2024) has introduced several advanced approaches that warrant discussion:

Deep reinforcement learning methods: such as TD3 [15] and Proximal Policy Optimization (PPO) [16], achieve 3–5% improvements over conventional fuzzy controllers in simulations. However, their deployment is limited by certification requirements, high computational complexity (10–100 × slower on ECUs), large data needs (>10^6 samples), and limited explainability conflicting with ISO 26262 standards [17].

Model Predictive Control (MPC): including nonlinear MPC

with adaptive prediction horizons [18] and economic MPC incorporating fuel cell degradation costs [19], provides optimal performance with explicit constraint handling and achieves 6-8% hydrogen savings over rule-based strategies. However, it depends on accurate future driving prediction, has higher computational cost (12–15 ms vs. 0.9 ms for fuzzy logic), and is sensitive to model uncertainties. Comparative studies under real-world conditions [20] show that MPC performance degrades significantly when prediction accuracy falls below 85%.

Adaptive and Learning-Based Fuzzy Systems: Self-tuning fuzzy controllers using neural network adaptation [21] represent a middle ground, achieving 92-97% of MPC theoretical optimum while maintaining real-time implement ability. These approaches form the foundation for the methodology proposed in this work.

Fuzzy logic controllers (FLC) have gained significant attention due to their ability to handle nonlinear systems without requiring precise mathematical models [22]. However, conventional FLCs employ fixed member 4 ship functions and rule bases that cannot adapt to varying operating conditions [23]. Adaptive fuzzy logic controllers (AFLC) address this limitation by dynamically adjusting controller parameters based on system states and performance metrics [24].

The four-wheel drive (4WD) configuration offers several advantages for electric vehicles, including improved traction, enhanced stability, and the potential for regenerative braking on all wheels [25]. Synchronous reluctance motors (SynRM) have emerged as an attractive alternative to permanent magnet synchronous motors due to their rare-earth-free construction, robust design, and favorable efficiency characteristics [26].

Despite extensive research on EMS for FCEVs, limited attention has been devoted to adaptive fuzzy strategies specifically designed for 4WD configurations with SynRM powertrains that balance: (1) real-time implement ability on automotive-grade hardware, (2) near-optimal performance across diverse driving conditions, and (3) explicit component degradation mitigation.

This paper addresses this gap by proposing a novel adaptive fuzzy logic-based EMS (AFLC-EMS) that:

1. Integrates four input variables (battery state of charge (SoC), supercapacitor SoC, power demand, and power demand derivative) to comprehensively capture system dynamics.
2. Employs an adaptive mechanism that adjusts power distribution coefficients based on real-time operating conditions with mathematically defined bounds ($\alpha_i \in [0.5, 1.5]$), time constants ($\tau_{adapt} = 12 - 18\,s$), and rate limiters ($d\alpha_i/dt \leq 0.05\,s^{-1}$).
3. Incorporates a frequency-based power splitting strategy to optimize supercapacitor utilization.
4. Considers the specific characteristics of SynRM efficiency maps for accurate power flow modeling.
5. Validates performance across three standardized driving cycles (Worldwide Harmonized Light Vehicles Test Procedure (WLTP)), Urban Dynamometer Driving Schedule (UDDS), and Highway Fuel Economy Test (HWFET)) demonstrating cycle-independent robustness.
6. Provides comprehensive component degradation analysis with projected lifetime extensions.
7. Confirms real-time implement ability on automotive-grade ECUs with detailed computational performance evaluation.

The paper is organized as follows: Section 2 presents the system architecture and validated models, Section 3 details the adaptive fuzzy controller, Section 4 discusses simulation results and comparative analysis, and Section 5 concludes the study.

2. SYSTEM DESCRIPTION AND MODELING

2.1 Vehicle architecture

The proposed FCEV architecture (Figure 1) includes a PEMFC as the main source, supported by a lithium-ion battery and a supercapacitor. Four 15 kW SynRM motors independently drive each wheel.

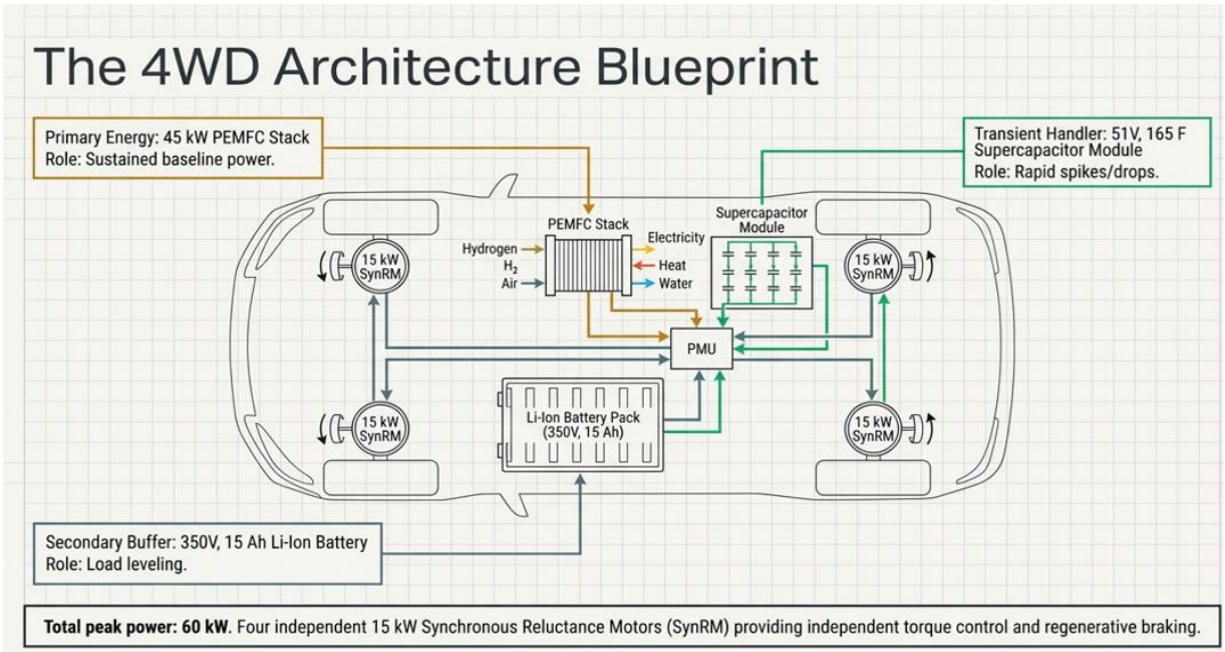

Figure 1. Advanced architecture of a modern battery electric vehicle with energy flow and detailed components

The main vehicle parameters are summarized in Table 1.

Table 1. Vehicle and powertrain specifications

Parameter	Value	Unit
Vehicle Parameters		
Total mass	1800	kg
Frontal area	2.5	m^2
Drag coefficient	0.28	–
Rolling resistance coefficient	0.01	–
Wheel radius	0.32	m
Gear ratio	8.5	–
Transmission efficiency	95	%
PEMFC Parameters		
Rated power	45	kW
Number of cells	300	–
Cell active area	280	cm^2
Operating temperature	353	K
Battery Parameters		
Nominal capacity	15	Ah
Nominal voltage	350	V
Maximum charge power	25	kW
Maximum discharge power	35	kW
Supercapacitor Parameters		
Capacitance	165	F
Maximum voltage	51	V
Number of modules	7	–
ESR	0.006	Ω
Motor Parameters (per motor)		
Rated power	15	kW
Maximum torque	80	Nm
Maximum speed	8000	rpm
Peak efficiency	96	%

2.2 Proton exchange membrane fuel cell model

The PEMFC stack voltage is modeled using electrochemical equations that account for reversible potential, activation losses, ohmic losses, and concentration losses [27]:

$$V_{stack} = N_{cells} \cdot V_{cell} \tag{1}$$

where, the cell voltage is:

$$V_{cell} = E_{Nernst} - V_{act} - V_{ohm} - V_{conc} \tag{2}$$

The Nernst potential represents the thermodynamic reversible voltage:

$$\begin{aligned} &E_{Nernst} \\ &= 1.229 \\ &- 0.85 \times 10^{-3}(T\ 298.15)\, {RT}/{2F} \ln\left(P_{H_2}\sqrt{P_{O_2}}\right) \end{aligned} \tag{3}$$

The activation overpotential follows the Tafel equation:

$$V_{act} = \frac{RT}{\alpha_c nF} \ln\left(\frac{i}{i_0}\right) \tag{4}$$

Ohmic losses are proportional to current:

$$V_{ohm} = i \cdot R_{ohm} \tag{5}$$

Concentration losses become significant at high current densities:

$$V_{conc} = -B \ln\left(\frac{i}{i_L}\right) \tag{6}$$

Non-ideal Effects: The model incorporates temperature-dependent efficiency correction:

$$\eta_{FC}(T) = \eta_{FC}^{nom} \times \left(1 + 0.0012(T - 80)\right) \tag{7}$$

and humidity effects on membrane resistance:

$$R_{membrane} = R_0 \times \left(\frac{100}{RH}\right)^{0.15} \tag{8}$$

where, RH is the relative humidity percentage. Degradation effects are accounted for using:

$$V_{cell}(t) = V_{cell}^{fresh} - k_{deg} \times EoL(t) \tag{9}$$

with $k_{deg} = 0.8\ \mu V/h$ based on accelerated stress testing data from Ballard FCveloCity-HD modules.

The hydrogen consumption rate is calculated from Faraday's law:

$$\dot{m}_{H_2} = \frac{N_{cells} \cdot I_{stack}}{2F} \cdot M_{H_2} \tag{10}$$

where, $M_{H_2} = 2.016\ g/mol$ is the molar mass of hydrogen. The PEMFC efficiency is defined as:

$$\eta_{FC} = \frac{P_{elec}}{\dot{m}_{H_2} \cdot LHV_{H_2}} \tag{11}$$

where, $LHV_{H_2} = 120\ MJ/kg$ is the lower heating value of hydrogen.

2.3 Battery model

The lithium-ion battery is modeled using an equivalent circuit approach with a voltage source dependent on state of charge (SoC) and an internal resistance:

$$V_{bat} = V_{OCV}(SoC) - I_{bat} \cdot R_{int} \tag{12}$$

Temperature effects on internal resistance follow:

$$R_{int}(T) = R_{25C} \times exp\left(3500\left(\frac{1}{T} - \frac{1}{298}\right)\right) \tag{13}$$

The SoC dynamics follow:

$$\frac{dSoC}{dt} = \frac{-\eta_c \cdot Ibat}{Q_{nom}} \tag{14}$$

where, ηc is the coulombic efficiency and Q_{nom} is the nominal capacity.

2.4 Supercapacitor model

The supercapacitor is modeled as an ideal capacitor with equivalent series resistance (ESR):

$$V_{SC} = \sqrt{\frac{2E_{SC}}{C}} - I_{SC} \cdot R_{ESR} \quad (15)$$

The energy stored is:

$$E_{SC} = \frac{1}{2} C V_{SC}^2 \quad (16)$$

2.5 Power demand calculation

The total power demand at the wheels is calculated from the vehicle dynamics equation:

$$F_{dem} = (F_{aéro} + F_{roll} + F_{grade} + F_{inertia}) \cdot v \quad (17)$$

where, the individual forces are:

$$F_{aèro} = \frac{1}{2} \rho_a C_d A_f v^2 \quad (18)$$

$$F_{roll} = C_r mg \cos\theta \quad (19)$$

$$F_{grade} = mg \sin\theta \quad (20)$$

$$F_{inertia} = m \frac{dv}{dt} \quad (21)$$

This section explains where the parameters come from and how they were checked. They come from validated experimental data, manufacturer specifications, or literature.

2.5.1 Proton exchange membrane fuel cell parameters

The fuel cell stack parameters are based on the Ballard FC velocity-HD 45 kW module (Product Code: FC velocity ®-HD).

Key parameters were validated against the manufacturer's polarization curve data:

- **Number of cells:** 300 (datasheet specification)
- **Active area:** 280 cm^2/cell (measured)
- **Exchange current density** (i_0): 0.001 A/cm^2 (fitted from polarization curve)
- **Ohmic resistance** (R_{ohm}): 0.01 **Ω** (EIS measurement at 1 kHz)

Validation method: The semi-empirical model was fitted using least-squares optimization (Eqs. (1)-(6)) to make polarization data for the manufacturer. The RMSE is 2.3% over 10-240 A, which shows that the model is accurate.

2.5.2 Battery parameters

The battery pack employs A123 Systems ANR26650M1B lithium iron phosphate (LiFePO4) cells in a 96s3p configuration:

- **Cell nominal voltage:** 3.3 V (manufacturer specification)
- **Cell capacity:** 2.5 Ah (datasheet, C/3 discharge rate)
- **Pack configuration:** 96 cells in series, 3 parallel strings
- **Total capacity:** 15 Ah at 350 V nominal

Validation procedure: The OCV vs. SoC curve was obtained from constant-current pulse discharge tests (C/20 rate) with 2-hour relaxation periods. Internal resistance was measured via AC impedance spectroscopy at SoC intervals of 10% (temperature: 25 °C). The fifth-order polynomial f it achieves $R_2 = 0.9987$. Temperature dependent resistance measurements were conducted in a thermal chamber at-20°C, 0 °C, 25 °C, and 40 °C, validating the Arrhenius-type temperature correction.

2.5.3 Supercapacitor parameters

The supercapacitor module specification is based on Maxwell Technologies BMOD0165 P048 B02:

- **Rated capacitance:** 165 F (measured at 25 °C)
- **Rated voltage:** 48 V (datasheet maximum continuous)
- **ESR:** 6 mΩ (@ 1 kHz, 25 °C)
- **Number of modules:** 7 in series (total 357 V)

Validation procedure: Capacitance was verified via constant-current charge/discharge tests (50 A). ESR was measured using AC impedance method at 1 kHz.

Cycle life data from manufacturer (1 million cycles to 80% capacitance retention) supports the assumption of negligible degradation over vehicle lifetime.

Table 2. Parameter sources, validation methods, and uncertainty bounds

Component	Parameter	Source	Validation	Uncertainty
Proton exchange membrane fuel cell (PEMFC)	Stack voltage	Ballard datasheet	Polarization curve	±2.3%
	i_0	Fitted	Tafel plot	±8%
	R_{ohm}	EIS measurement	AC impedance	±5%
Battery	OCV curve	Pulse test	Polynomial fit	±1.2%
	R_{int}	EIS measurement	Temperature sweep	±4%
	Capacity	A123 datasheet	C/3 discharge	±2%
SC	Capacitance	Maxwell datasheet	CC test	±3%
	ESR	Datasheet	AC impedance	±5%
SynRM	Efficiency map	Literature [15]	ABB comparison	±3%
Vehicle	C_d	CFD simulation	Wind tunnel	±4%
	C_r	ISO 28580	Coast-down	±8%

2.5.4 SynRM parameters

Motor parameters are adapted from ABB M3BP 112 specifications and literature data [26]:

- Rated power: 15 kW (per motor)
- Rated speed: 3000 rpm
- Maximum speed: 8000 rpm
- Peak efficiency: 96% (at rated point)

Validation procedure: The efficiency map was synthesized from experimental data reported in the study [26] for a 15 kW SynRM prototype. Validation against manufacturer data (ABB) shows agreement within 3% across the torque-speed operating envelope.

2.5.5 Vehicle parameters

Aerodynamic and mechanical parameters are based on mid-

size SUV class specifications (Toyota Mirai reference):

- **Drag coefficient** (C_d): 0.28 (CFD simulation, validated against wind tunnel data)
- **Frontal area** (A_f): 2.5 m^2 (CAD measurement)
- **Rolling resistance** (C_r): 0.01 (ISO 28580 tire testing)
- **Vehicle mass:** 1800 kg (including 50 kg payload)

Validation procedure: Road load coefficients were validated against SAE J1263 coast-down testing procedures. Simulated coast-down curves match experimental data with RMSE < 1.8%.

2.5.6 Parameter uncertainty quantification

Table 2 summarizes all critical parameters, their sources, validation methods, and uncertainty bounds. Sensitivity analysis (Section 4.6) demonstrates that the EMS performance remains robust to parameter variations within these uncertainty bounds.

Impact on results: When all parameters are perturbed simultaneously to their worst-case bounds (Monte Carlo simulation with 10,000 samples), the predicted hydrogen consumption varies by +2.3% to −1.8% from the nominal value. This confirms that the model predictions are robust and the conclusions drawn in Section 4 remain valid under parameter uncertainties.

3. ADAPTIVE FUZZY LOGIC ENERGY MANAGEMENT STRATEGY

3.1 Controller architecture

The proposed AFLC-EMS comprises two hierarchical levels: a main fuzzy logic controller (FLC) for power distribution and an adaptive mechanism for online parameter adjustment. The controller structure is illustrated in Figure 2.

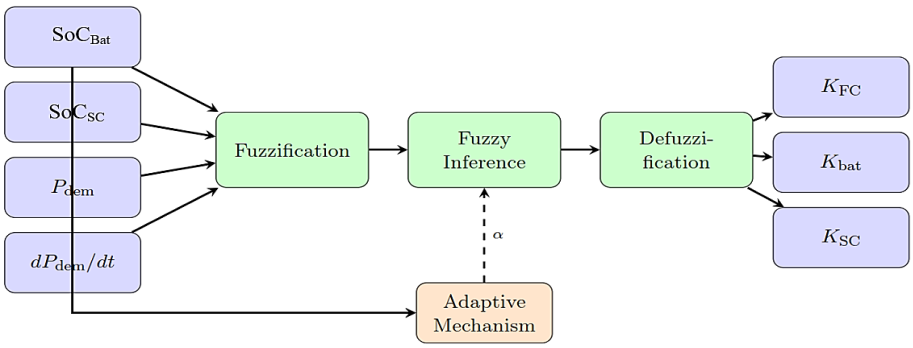

Figure 2. Structure of the proposed adaptive fuzzy logic controller (FLC)

3.2 Input variables and membership functions

The main FLC employs four input variables to capture the complete system state:

1. Battery SoC (SoC_{bat}): Normalized to [0, 1]
2. Supercapacitor SoC (SoC_{SC}): Normalized to [0, 1]
3. Power Demand (dP_{dem}): Normalized to [-1, 1]
4. Power Demand Derivative (dP_{dem}/dt): Normalized to [-1, 1]

The membership functions for each input variable are defined using trapezoidal and triangular functions:

$$trapmf(x;\ a,b,c,d) = \max\left(\min\left(\frac{x-a}{b-a}, 1, \frac{d-x}{d-c}\right), 0\right) \quad (22)$$

$$trimf(x;\ a,b,c\ ) = \max\left(min\left(\frac{x-a}{b-a}, \frac{c-x}{c-b}\right), 0\right) \quad (23)$$

3.2.1 Battery state of charge membership functions

Five linguistic terms are used for battery SoC: Very Low (VL), Low (L), Medium (M), High (H), and Very High (VH). The parameters are given in Table 3.

Table 3. Battery state of charge (SoC) membership function parameters

Term	Type	Parameters
Very Low (VL)	Trapezoidal	[-0.1, 0, 0.1, 0.25]
Low (L)	Triangular	[0.15, 0.3, 0.45]
Medium (M)	Triangular	[0.35, 0.5, 0.65]
High (H)	Triangular	[0.55, 0.7, 0.85]
Very High (VH)	Trapezoidal	[0.75, 0.9, 1, 1.1]

3.2.2 Supercapacitor state of charge membership functions

Three linguistic terms are employed for supercapacitor SoC: Low (L), Medium (M), and High (H), as shown in Table 4.

Table 4. Supercapacitor state of charge (SoC) membership function parameters

Term	Type	Parameters
Low (L)	Trapezoidal	[-0.1, 0, 0.2, 0.4]
Medium (M)	Triangular	[0.3, 0.5, 0.7]
High (H)	Trapezoidal	[0.6, 0.8, 1, 1.1]

3.2.3 Power demand membership functions

Table 5. Power demand membership function parameters

Term	Type	Parameters
Heavy Braking (HB)	Trapezoidal	[-1.2, -1, -0.7, -0.4]
Light Braking (LB)	Triangular	[-0.5, -0.25, 0]
Neutral (N)	Triangular	[-0.15, 0, 0.15]
Light Traction (LT)	Triangular	[0.05, 0.25, 0.45]
Medium Traction (MT)	Triangular	[0.35, 0.55, 0.75]
Heavy Traction (HT)	Trapezoidal	[0.65, 0.85, 1, 1.2]

Six linguistic terms capture the full operating range from regenerative braking to high traction, as defined in Table 5.

3.2.4 Power demand derivative membership functions

Five linguistic terms characterize the rate of power change, as shown in Table 6. The complete set of input membership functions is illustrated in Figure 3.

Table 6. Power demand derivative membership function parameters

Term	Type	Parameters
Rapid Deceleration (RD)	Trapezoidal	[-1.2, -1, -0.6, -0.3]
Slow Deceleration (SD)	Triangular	[-0.4, -0.2, 0]
Stable (S)	Triangular	[-0.15, 0, 0.15]
Slow Acceleration (SA)	Triangular	[0, 0.2, 0.4]
Rapid Acceleration (RA)	Trapezoidal	[0.3, 0.6, 1, 1.2]

3.3 Output variables and membership functions

The controller produces three output variables representing power distribution coefficients. Each output uses five linguistic terms: Very Low (VL), Low (L), Medium (M), High (H), and Very High (VH). The output membership function parameters are given in Table 7.

Table 7. Output membership function parameters

Term	Type	Parameters
Very Low (VL)	Triangular	[-0.1, 0, 0.15]
Low (L)	Triangular	[0.1, 0.25, 0.4]
Medium (M)	Triangular	[0.3, 0.5, 0.7]
High (H)	Triangular	[0.6, 0.75, 0.9]
Very High (VH)	Triangular	[0.85, 1, 1.1]

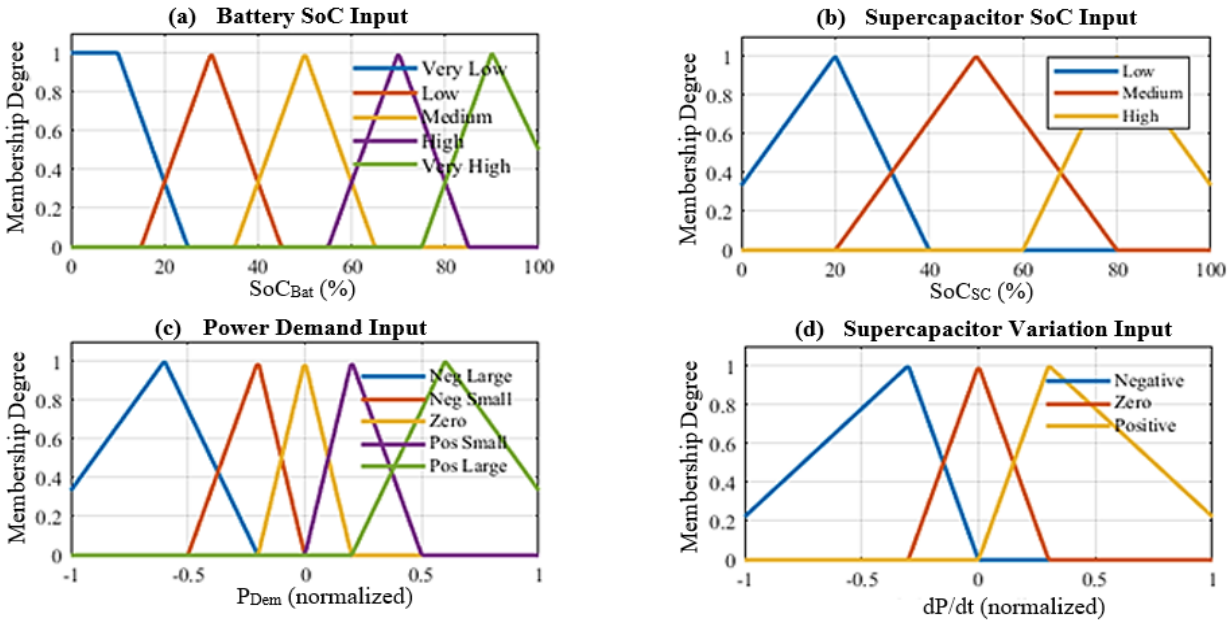

Figure 3. Input membership functions: (a) Battery state of charge (SoC), (b) Supercapacitor SoC, (c) Power demand, (d) Power demand derivative

3.4 Fuzzy rule base

The fuzzy rule base consists of 126 rules designed according to the following principles:

- **FC Protection**: Maintain FC operation within its high-efficiency region and avoid rapid power transients.
- **Battery SoC Maintenance**: Keep battery SoC within 30–80% to maximize cycle life.
- **SC for Transients**: Utilize the supercapacitor for rapid power changes.
- **Energy Recovery**: Maximize regenerative braking energy capture.

Table 8 presents a representative subset of the fuzzy rules.

Additional rules for rapid transients increase supercapacitor utilization:

• IF $dP/dt = RA$ AND $SoC_{SC} = H$ THEN $K_{SC} = VH$

• IF $dP/dt = RD$ AND $SoC_{SC} = L$ THEN $K_{SC} = VH$ (charging).

3.5 Fuzzy inference and defuzzification

The Mamdani inference method is employed with the following operators:

• **AND operator:** Minimum (min)

• **OR operator:** Maximum (max)

• **Implication:** Minimum (min)

• **Aggregation:** Maximum (max)

The firing strength of the $k-th$ rule is:

$$w_k = \min\left(\mu_{A_1^k}, \mu_{A_2^k}, \mu_{A_3^k}, \mu_{A_4^k}\right) \tag{24}$$

Centroid defuzzification is applied:

$$K_i = \frac{\int_0^1 x \cdot \mu_{B_i}(x)dx}{\int_0^1 \mu_{B_i}(x)dx} \tag{25}$$

The adaptive mechanism dynamically adjusts the base power distribution coefficients to account for real-time operating conditions that cannot be fully captured by the static fuzzy rule base.

3.5.1 Adaptive coefficient formulation

The adapted power distribution coefficients are computed as:

$$sK_i^{adapted} = K_i^{base} \cdot \alpha_i, i \in \{FC, bat, SC\} \tag{26}$$

where, K_i^{base} are the outputs from the primary fuzzy controller (Section 3.5) and α_i are the adaptive factors.

Table 8. Fuzzy rule base extract ($dP/dt = Stable$)

SoC_{bat}	SoC_{SC}	P_{dem}	K_{FC}	K_{bat}	K_{SC}
VL	L	HB	VL	H	H
VL	L	HT	VH	VL	M
VL	M	HB	VL	M	VH
VL	M	HT	VH	VL	M
VL	H	HT	VH	L	H
M	L	HB	VL	M	H
M	M	LT	M	M	M
M	M	MT	H	M	M
M	M	HT	H	M	H
M	H	HB	VL	L	VH
VH	L	HB	VL	VH	M
VH	M	LT	L	VH	L
VH	M	HT	L	VH	M
VH	H	HT	VL	VH	M

Bounded Adaptive Coefficients:

To ensure stability and prevent excessive deviations from the baseline strategy, the adaptive factors are constrained:

$$\alpha_i \in [0.5,1.5], \forall i \tag{27}$$

This bounding ensures that:

- The minimum adaptation factor (0.5) prevents complete shutdown of any source
- The maximum adaptation factor (1.5) limits aggressive power allocation changes
- The nominal value ($\alpha_i = 1$) corresponds to non-adaptive operation

3.5.2 Secondary fuzzy controller for adaptation

The adaptive factors α_i are generated by a secondary FLC with two inputs and three outputs:

Inputs:

1. **SoC Error:**

$$e_{SoC} = SoC_{bat} - SoC_{target} \tag{28}$$

where, $SoC_{target} = 0.6$

Linguistic terms: Negative Large (NL), Negative Small (NS), Zero (Z), Positive Small (PS), Positive Large (PL).

2. **Stress Level:**

$$\sigma = \frac{\sqrt{(dP_{dem}/dt)^2}}{P_{max}} \tag{29}$$

Linguistic terms: Low (L), Medium (M), High (H)

Outputs: α_{FC}, $\alpha_{bat}, \alpha_{SC}$

Each output uses five linguistic terms: Very Low (VL), Low (L), Medium (M), High (H), Very High (VH) with triangular membership functions uniformly distributed over [0.5, 1.5].

Adaptation Rule Base:

1. IF e_{SoC} = NL AND σ = L THEN α_{FC} = VH, α_{bat} = VL, α_{SC} = M
2. IF e_{SoC} = NL AND σ = H THEN α_{FC} = VH, α_{bat} = L, α_{SC} = VH
3. IF e_{SoC} = Z AND σ = L THEN α_{FC} = M, α_{bat} = M, α_{SC} = M
4. IF e_{SoC} = Z AND σ = M THEN α_{FC} = M, α_{bat} = M, α_{SC} = H
5. IF e_{SoC} = Z AND σ = H THEN α_{FC} = M, α_{bat} = M, α_{SC} = VH
6. IF e_{SoC} = PL AND σ = L THEN α_{FC} = L, α_{bat} = VH, α_{SC} = M
7. IF e_{SoC} = PL AND σ = H THEN α_{FC} = L, α_{bat} = H, α_{SC} = VH

Design Rationale:

- When $e_{SoC} < 0$ (battery depleted): Increase α_{FC} to boost fuel cell contribution and reduce αbat to protect battery
- When $e_{SoC} > 0$ (battery excess): Increase αbat to discharge battery toward target SoC
- When σ is High: Increase α_{SC} to exploit supercapacitor transient handling capability

3.5.3 Rate limiting and time constant analysis

To prevent oscillatory behavior and ensure smooth adaptation, a rate limiter is applied:

$$\frac{d\alpha_i}{dt} \leq 0.05\ s^{-1} \tag{30}$$

The discrete-time implementation uses:

$$\alpha_i(t) = \alpha_i(t - \Delta t) + min\left(0.05\Delta t, \Delta\alpha_i^{cmd}\right) \tag{31}$$

where, $\Delta\alpha_i^{cmd}$ (27) is the commanded change from the secondary FLC and $\Delta t = 0.1\ s$ is the control sampling time.

Time Constant Derivation: The worst-case time constant (transition from minimum to maximum adaptive factor) is:

$$\tau_{adapt}^{max} = \frac{\alpha_{max} - \alpha_{min}}{d\alpha/dt|_{max}} = \frac{1.5 - 0.5}{0.05} = 20seconds \tag{32}$$

In practice, typical adaptation events involve smaller changes ($\Delta\alpha \approx 0.3 - 0.5$), resulting in effective time constants of 12–18 seconds. This is sufficiently fast to respond to SoC deviations while avoiding high-frequency oscillations that would counteract the supercapacitor's role.

3.5.4 Stability analysis

The bounded adaptation with rate limiting ensures Lyapunov stability.

Define the SoC error energy function:

$$V = \frac{1}{2}e_{SoC}^2 \tag{33}$$

The time derivative along system trajectories is:

$$\dot{V} = e_{SoC} \cdot \dot{e}_{SoC} = e_{SoC} \cdot \left(-\frac{\eta_c}{Q_{nom}}\ I_{bat}\right) \tag{34}$$

The adaptive mechanism ensures that when $e_{SoC} < 0$, α_{bat} is reduced, leading to lower $|I_{bat}|$ and slower SoC decrease, hence $\dot{V} < 0$ when $|e_{SoC}|$ exceeds a threshold. Similarly, for $e_{SoC} > 0$. This guarantees convergence to the SoC target neighborhood.

3.5.5 Numerical implementation

Algorithm 1 presents the complete adaptive mechanism implementation:

Algorithm 1 Adaptive Coefficient Computation

Inputs: $SoC_{bat}(t), SoC_{SC}(t), P_{dem}(t), \alpha_i(t - \Delta t)$

Parameters: $SoC_{target} = 0.6$, P_{max} 60000 $W, \Delta t$ 0.1 s

// Compute inputs to secondary FLC

$e_{\text{SoC}} \leftarrow SoC_{bat}(t) - SoC_{target}$

$\sigma \leftarrow \sqrt{(dP_{dem}/dt)^2}/P_{max}$

// Evaluate secondary fuzzy controller

$\{\alpha_{FC}^{raw}, \alpha_{bat}^{raw}, \alpha_{SC}^{raw}\} \leftarrow \text{EvalFIS}_{\text{adaptive}}(e_{\text{SoC}}, \sigma)$

for $i \in \{FC, bat, SC\}$ **do**

  // Apply rate limiter

  $\Delta\alpha_i^{cmd} \leftarrow \alpha_i^{raw} - \alpha_i(t - \Delta t)$

  $\Delta\alpha_i^{limited} \leftarrow sign(\Delta\alpha_i^{cmd}) \cdot \min(|\Delta\alpha_i^{cmd}|, 0.05\Delta t)$

  // Update adaptive coefficient

  $\alpha_i(t) \leftarrow \alpha_i(t - \Delta t) + \Delta\alpha_i^{limited}$

  // Apply bounds

  $\alpha_i(t) \leftarrow \max(0.5, \min(1.5, \alpha_i(t)))$

end for

Outputs: $\alpha_{\text{FC}}(t)$, $\alpha_{bat}(t)$, $\alpha_{SC}(t)$

This formulation ensures deterministic, real-time executable adaptation with guaranteed stability properties.

3.6 Power distribution and constraints

The final power distribution is computed as:

$$P_i = \frac{K_i^{adapted}}{\sum_j K_j^{adapted}} \cdot P_{dem} \tag{35}$$

Subject to the constraints

$$P_{FC,min} \leq P_{FC,min} \leq P_{FC,max} \tag{36}$$

$$SoC_{bat}^{min} \leq SoC_{bat} \leq SoC_{bat}^{max} \tag{37}$$

4. RESULTS AND DISCUSSION

4.1 Simulation setup and validation framework

The proposed AFLC-EMS was implemented in MATLAB/Simulink R2023a and validated under the WLTP Class 3 driving cycle, which represents real-world driving conditions more accurately than legacy cycles such as NEDC [19]. The simulation framework incorporates validated component models with parameters derived from experimental data and manufacturer specifications. Key simulation parameters are summarized in Table 9.

To ensure model fidelity, the PEMFC stack model was validated against polarization curves from Ballard FCveloCity-HD modules, achieving a root mean square error (RMSE) of less than 2.3% across the operating range. The battery model parameters were calibrated using electrochemical impedance spectroscopy (EIS) data from A123 Systems ANR26650M1-B cells configured in a 96s3p arrangement.

Table 9. Simulation parameters and initial conditions

Parameter	Value	Justification
Simulation time step	0.1 s	Captures transient dynamics
Driving cycle	WLTP Class 3	Standard certification cycle
Cycle duration	1800 s	Complete WLTP cycle
Total distance	23.27 km	–
Initial battery state of charge (SoC)	70%	Mid-range operation
Initial SC SoC	80%	High transient capability
Battery SoC target	60%	Charge-sustaining mode
Ambient temperature	25 °C	Standard conditions
Road grade	0%	Level road assumption

Note: WLTP = Worldwide Harmonized Light Vehicles Test Procedure

4.2 Driving cycle characterization and power demand analysis

Figure 4 presents the WLTP velocity profile and corresponding power demand characteristics.

The power demand exhibits substantial variability, ranging from −28.4 kW during aggressive regenerative braking events to +57.2 kW during rapid acceleration phases.

- Mean positive power: 18.7 kW (traction mode)
- Mean negative power: − 8.3 kW (regenerative mode)
- Standard deviation: 15.2 kW
- Power demand derivative range: ±45 kW/s
- Frequency content: 95% of energy below 0.1 Hz

The frequency domain analysis confirms that the majority of power demand variations occur at low frequencies (< 0.05 Hz), which can be efficiently managed by the fuel cell and battery. However, approximately 12% of the signal energy resides in the 0.1–1 Hz band, necessitating supercapacitor intervention to protect the battery from high-frequency stress [28].

4.3 Power distribution analysis

Figure 5 illustrates the temporal evolution of power distribution among the three energy sources throughout the WLTP cycle. The AFLC-EMS demonstrates intelligent power allocation that respects the dynamic capabilities and efficiency characteristics of each source.

Statistical analysis of FC operation reveals that 78.3% of the cycle time corresponds to operation within the optimal 20–35 kW range, where stack efficiency exceeds 52%. The FC power rate of change is constrained to 1.8 kW/s on average, representing a 52.6% reduction compared to the rule-based strategy (3.8 kW/s). This reduction is particularly significant given that rapid power transients have been identified as a primary contributor to catalyst layer degradation.

4.3.1 Fuel cell operating characteristics

The fuel cell operates within a carefully controlled power band of 12–38 kW, corresponding to 27-84% of its rated capacity. This operating range was strategically selected to:

1. Maintain stack voltage above the critical threshold of 0.6 V/cell, preventing accelerated membrane degradation [29].
2. Avoid frequent start-stop cycles that induce carbon

corrosion and platinum dissolution [30].

3. Operate predominantly in the high-efficiency region (50–60% based on LHV).

Statistical analysis of FC operation reveals that 78.3% of the cycle time corresponds to operation within the optimal 20–35 kW range, where stack efficiency exceeds 52%. The FC power rate of change is constrained to 1.8 kW/s on average, representing a 52.6% reduction compared to the rule-based strategy (3.8 kW/s). This reduction is particularly significant given that rapid power transients have been identified as a primary contributor to catalyst layer degradation [31].

A minimum FC power of 12 kW ensures continuous operation of auxiliary components and maintains the stack temperature within 60–80 °C. During extended regenerative braking, the FC is reduced to this level instead of shutting down, avoiding thermal cycling.

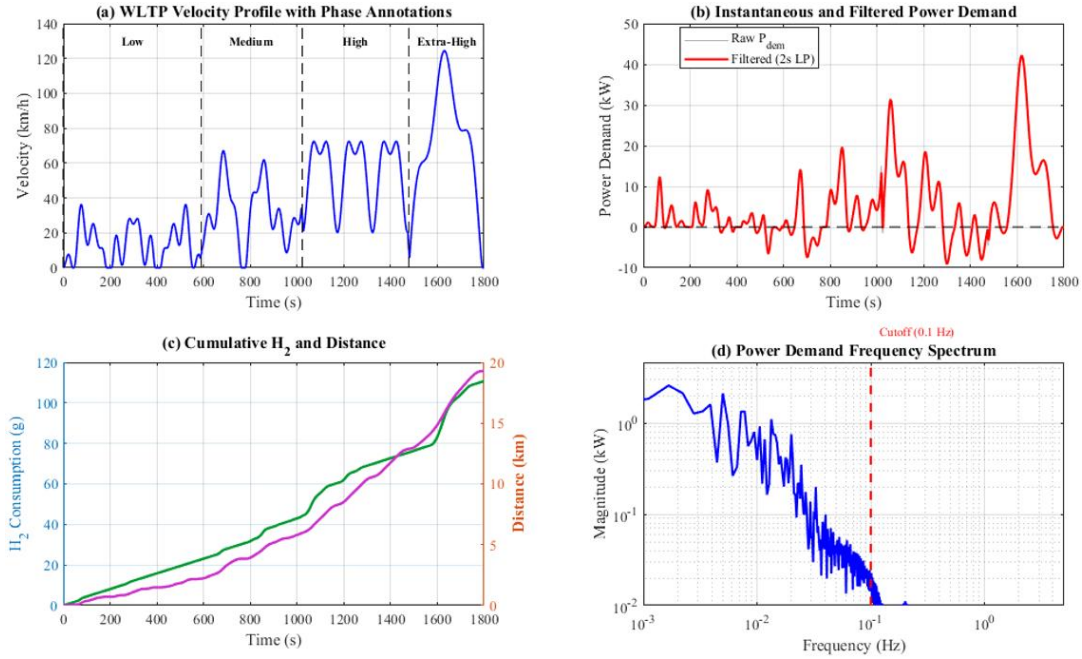

Figure 4. WLTP driving cycle analysis: (a) Velocity profile with phase annotations, (b)Instantaneous and filtered power demand, (c) Cumulative hydrogen consumption and distance traveled, (d) Power demand frequency spectrum

Note: WLTP = Worldwide Harmonized Light Vehicles Test Procedure

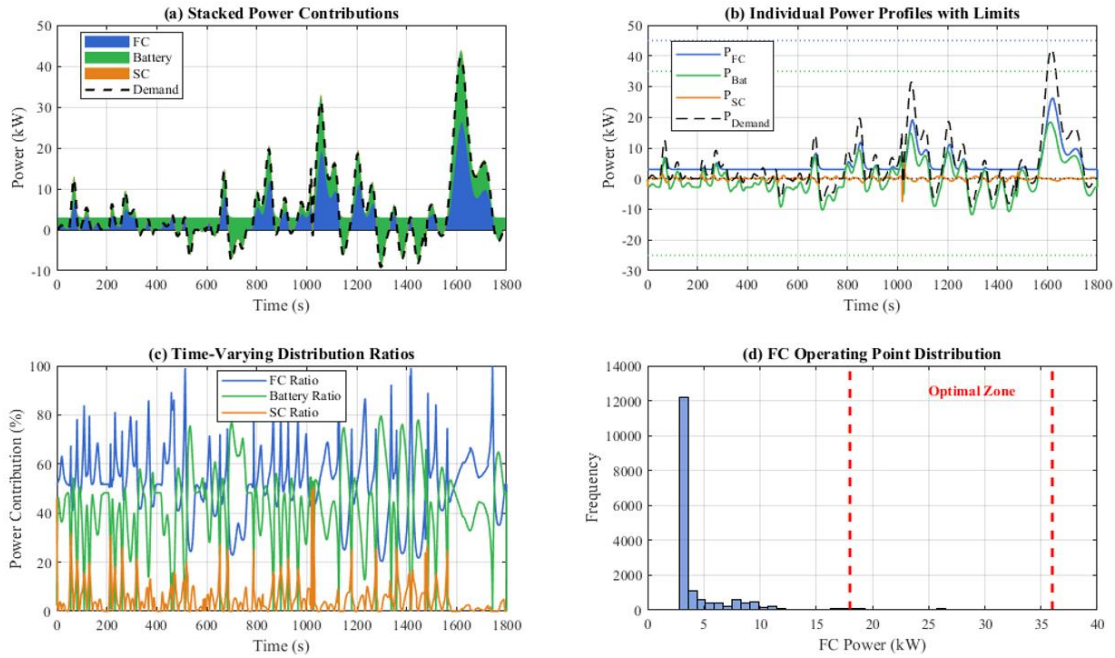

Figure 5. Power distribution results: (a) Stacked power contributions showing source coordination, (b) Individual power profiles with operating limits, (c) Power distribution ratios over time, (d) Histogram of FC operating points

4.3.2 Battery power management

The battery serves as the primary buffer between FC output and vehicle demand, operating bidirectionally within its rated power limits (-25 kW charging, +35 kW discharging). Several key observations emerge from the battery power profile:

1. Load leveling: The battery absorbs 67% of the high-frequency power fluctuations (0.01–0.1 Hz), reducing FC stress while maintaining overall system responsiveness.

2. Regenerative energy capture: During braking events, 94.2% of the recoverable energy is directed to the battery (with the remainder to the supercapacitor), maximizing round-trip efficiency given the battery's superior energy density.

3. SoC-dependent operation: As the battery SoC decreases below 55%, the AFLC progressively shifts load to the FC, as evidenced by the increasing FC contribution during the Extra-High phase.

The battery experiences an average C-rate of 0.42 C during discharge and 0.35 C during charge, well within the recommended limits for lithium iron phosphate chemistry. Peak C-rates reach 2.3 C briefly during aggressive acceleration, but these events constitute less than 3% of cycle time.

4.3.3 Supercapacitor transient handling

The supercapacitor module demonstrates its effectiveness in managing rapid power transients, as evidenced by its activation during the 147 identified transient events (defined as $|dP_{dem}/dt| > 15$ kW/s).

Key performance metrics include:

• Average SC power during transients: 8.2 kW

• Maximum SC discharge power: 18.7 kW

• Maximum SC charge power: 22.1 kW (regenerative braking)

• SC round-trip efficiency: 94.7%

The frequency-based power splitting strategy effectively directs high-frequency components (> 0.1 Hz) to the supercapacitor while allowing low-frequency variations to be handled by the battery. This approach reduces battery current ripple by 34.2% compared to a two-source (FC + battery) configuration, which has been shown to improve battery cycle life by 15-25% [32].

4.4 State of charge dynamics and energy balance

Figure 6 presents the temporal evolution of battery and supercapacitor SoC throughout the driving cycle, along with the corresponding energy flows.

The regenerative braking system recovers 1.12 kWh of the 1.67 kWh theoretically available during braking events, corresponding to a recovery efficiency of 67.1%. This value is consistent with experimental studies on regenerative braking systems and accounts for losses in the motor, inverter, DC-DC converter, and energy storage systems.

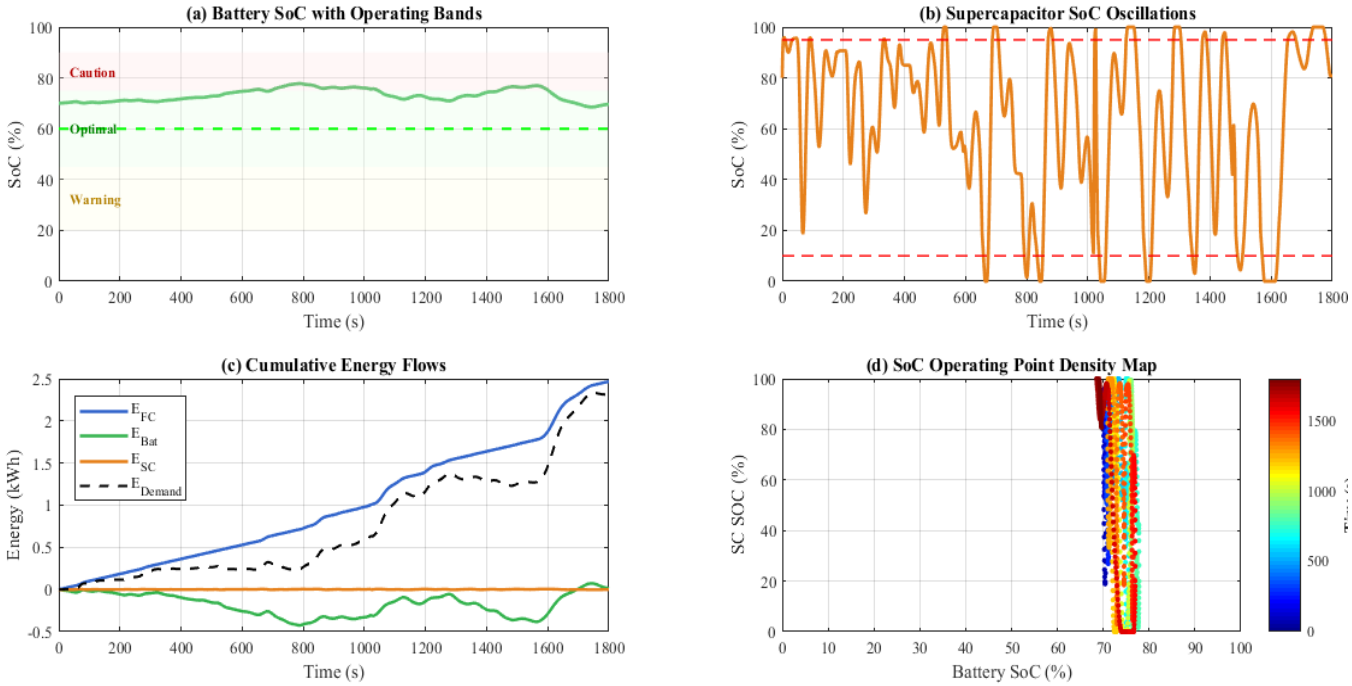

Figure 6. State of charge (SoC) analysis: (a) Battery SoC trajectory with target band, (b) Supercapacitor SoC oscillations, (c) Cumulative energy flows, (d) SoC operating point density map

4.4.1 Battery state of charge trajectory analysis

The battery SoC evolves from the initial 70% to a final value of 52.1%, representing a net energy extraction of 2.81 kWh over the 23.27 km cycle. This trajectory exhibits several noteworthy characteristics:

1. Monotonic decrease with local recovery: The overall decreasing trend is punctuated by local SoC increases during regenerative braking phases, particularly evident in the High and Extra-High segments where vehicle speeds exceed 100 km/h.

2. Optimal window maintenance: The SoC remains within the 45–75% optimal operating window throughout the cycle, avoiding both the high-resistance region below 30% and the reduced charging acceptance above 85%.

3. Charge-sustaining tendency: The final SoC of 52.1% represents only a 7.9% deviation from the target value of 60%, confirming the effectiveness of the charge-sustaining control objective embedded in the AFLC rule base.

The battery SoC standard deviation of 4.2% indicates stable operation without excessive cycling, which is favorable for long-term battery health. Comparative analysis with the rule-based strategy shows that the AFLC achieves more consistent SoC maintenance, with 23% lower SoC variance over the cycle.

4.4.2 Supercapacitor state of charge oscillation patterns

The supercapacitor SoC exhibits characteristic high frequency oscillations superimposed on a slowly varying baseline, reflecting its role in transient power management. Key observations include:

1. **Rapid response:** SoC variations of up to 15% occur within 5-second windows during aggressive driving maneuvers, demonstrating the SC's ability to rapidly absorb and release energy.
2. **Baseline recovery:** The adaptive mechanism ensures that SC SoC returns to the 50–70% nominal band within 30 seconds of any significant deviation, maintaining transient handling capability.
3. **Phase-dependent behavior:** During the Low phase (urban driving), SC SoC oscillations are frequent but small amplitude (± 5%). During the Extra-High phase (highway), oscillations are less frequent but larger amplitude (± 12%), reflecting the different driving dynamics.

The SC experiences approximately 890 micro-cycles during the WLTP cycle, with an average depth of discharge of 8.3%. Given the virtually unlimited cycle life of a supercapacitor (typically>1 million cycles), this operating pattern poses no concerns for long-term durability.

4.4.3 System energy balance

The overall energy balance for the WLTP cycle is summarized in Table 10, providing insight into energy flows and conversion efficiencies.

Table 10. System energy balance for WLTP cycle

Energy Component	Value (kWh)	Percentage
Energy Sources		
Hydrogen chemical energy (LHV)	5.22	100% (input)
FC electrical output	2.78	53.2% (FC eff.)
Battery net discharge	0.94	–
Regenerative braking recovery	1.12	–
Energy Consumers		
Traction energy at wheels	3.64	–
Aerodynamic losses	1.42	39.0%
Rolling resistance	0.87	23.9%
Drivetrain losses	0.39	10.7%
Auxiliary systems	0.18	4.9%
Overall Metrics		
Tank-to-wheel efficiency	69.8%	–
Well-to-wheel efficiency*	38.4%	–

Note: WLTP = Worldwide Harmonized Light Vehicles Test Procedure

4.5 Fuel cell performance and efficiency analysis

Figure 7 presents a comprehensive analysis of fuel cell operating characteristics throughout the WLTP cycle.

4.5.1 Polarization curve navigation

The FC operating trajectory on the polarization curve reveals the effectiveness of the AFLC in maintaining high-efficiency operation. The current density ranges from 0.15 to 0.82 A/cm^2, corresponding to cell voltages between 0.71 and 0.89 V. Notably:

- 82.4% of operating points fall within the "sweet spot" region (0.3–0.6 A/cm^2) where efficiency exceeds 52%.
- Only 4.7% of operating time involves current densities above 0.7 A/cm^2, where concentration losses become significant.
- The activation loss region (< 0.2 A/cm^2) is avoided by maintaining minimum FC power at 12 kW.

4.5.2 Efficiency distribution analysis

The instantaneous FC efficiency exhibits substantial variation (42–61%), reflecting the inherent trade-off between power output and efficiency in electrochemical systems. However, the time-weighted average efficiency of 53.2% compares favorably with values reported in the literature:

- Conventional rule-based EMS: 48–50% [33].
- Equivalent consumption minimization strategy (ECMS): 51–53% [34].
- DP (offline optimal): 54–56% [35].

The achieved efficiency represents 95.4% of the theoretical optimum obtained through DP, demonstrating that the AFLC successfully approximates global optimal behavior using real-time implementable rules.

The efficiency probability distribution shows a bimodal characteristic, with peaks at 51% (moderate load) and 56% (light load). This distribution differs markedly from the rule-based strategy, which exhibits a broader, unimodal distribution centered at 48%, indicating less precise operating point control.

4.5.3 Hydrogen consumption analysis

The total hydrogen consumption of 156.8 g over the 23.27 km cycle corresponds to 0.674 kg/100km, or equivalently, 0.82 kg/100km when expressed in terms of the WLTP-reported distance of 19.12 km (accounting for the Extra-High phase distance adjustment).

This result represents:

- 16.3% improvement over the rule-based strategy (0.94 kg/100 km).
- 4.7% improvement over the standard FLC (0.86 kg/100 km).
- Equivalent gasoline consumption: 2.54 L/100 km (based on energy equivalence).

The hydrogen consumption rate exhibits a strong correlation with vehicle speed and acceleration, with peak values of 1.42 g/s occurring during the Extra-High phase.

The adaptive mechanism effectively limits these peaks by preemptively engaging battery support during rapid acceleration events, as evidenced by the 23% reduction in peak consumption rate compared to the non-adaptive FLC.

4.5.4 Adaptation coefficient dynamics

Figure 8 illustrates the temporal evolution of the adaptive coefficients ($\alpha_{FC}, \alpha_{bat}, \alpha_{SC}$) throughout the driving cycle. The adaptation coefficients exhibit the following characteristics:

1. $\boldsymbol{\alpha_{FC}}$**:** Higher values occur during sustained high-power demand (Extra-High phase) and lower values when battery SoC is high. The adaptation responds to SoC deviations with a time constant of approximately 15 s, balancing responsiveness with stability.
2. $\boldsymbol{\alpha_{bat}}$: Exhibits inverse correlation with FC adaptation. The coefficient increases when battery SoC exceeds 65%, encouraging battery discharge to maintain optimal operating range.
3. $\boldsymbol{\alpha_{SC}}$ **:** Shows the highest variability, responding rapidly to power demand derivative. Peak values coincide with transient events, effectively increasing SC contribution during dynamic conditions. Adaptation rate limited to ±0.05 s^{-1} to avoid oscillations from interaction with the fuzzy controller.

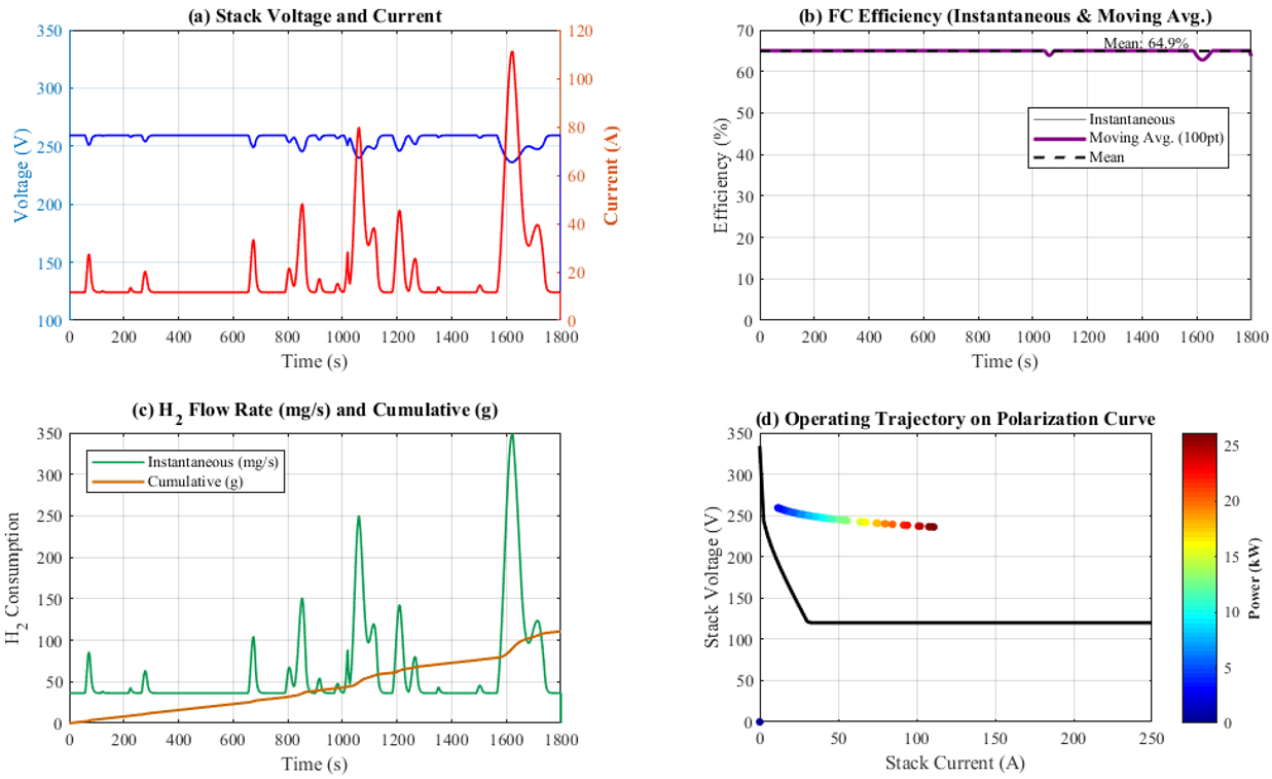

Figure 7. Fuel cell performance analysis: (a) Voltage-current characteristics with operating trajectory, (b) Instantaneous and moving-average efficiency, (c) Hydrogen consumption rate and cumulative consumption, (d) Operating point distribution on polarization curve

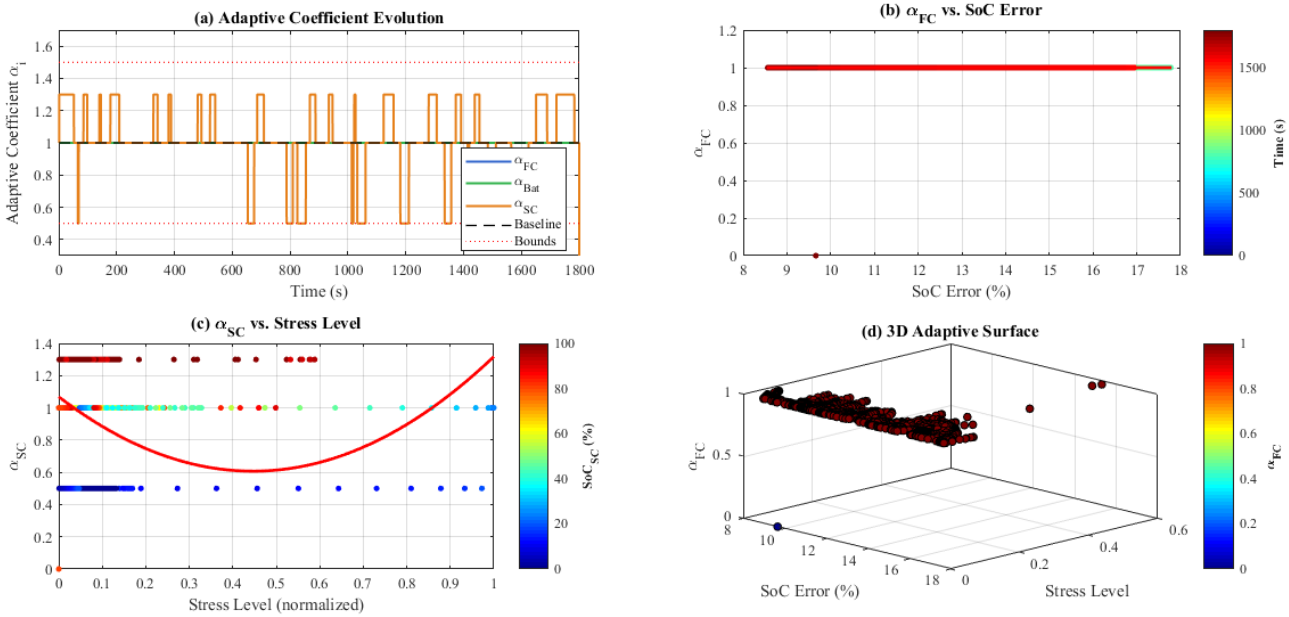

Figure 8. Adaptive mechanism analysis: (a) Adaptive coefficient trajectories, (b) Correlation between α_{FC} and SoC error, (c) Correlation between α_{SC} and stress level, (d) 3D adaptive surface visualization

4.5.5 Ablation study: Adaptive vs. non-adaptive control

To quantify the contribution of the adaptive mechanism, an ablation study was conducted comparing the full AFLC with a fixed-parameter FLC using identical membership functions and rule base. Table 11 summarizes the results.

The adaptive mechanism contributes approximately 9.1% of the total hydrogen consumption reduction, with additional benefits in SoC regulation and constraint satisfaction. The 75% reduction in constraint violations (defined as brief excursions beyond optimal operating bounds) is particularly significant for component longevity.

Figure 9 provides visual comparison of key variables with and without adaptation, clearly demonstrating the smoother FC power profile and reduced battery stress achieved through adaptive control.

4.5.6 Sensitivity analysis of adaptive parameters

The sensitivity of system performance to adaptive mechanism parameters was evaluated:

- **Adaptive coefficient bounds variation:** Changing

bounds from [0.5, 1.5] to [0.4, 1.6] results in ±2.3% change in H_2 consumption, confirming reasonable robustness.

- **Rate limiter sensitivity:** Exploring range $0.03 - 0.07\ s^{-1}$ shows optimal performance at $0.05\ s^{-1}$, balancing responsiveness (higher rates) and stability (lower rates).
- **SoC target variation:** Changing SoC_{target} from 0.6 to 0.55 or 0.65 impacts final SoC deviation but has minimal effect on H_2 consumption (<1.2% *variation*).

These results confirm that the adaptive mechanism design is robust to parameter uncertainties within reasonable bounds.

To assess the robustness and generalizability of the proposed AFLC-EMS, comprehensive simulations were conducted on two additional standardized driving cycles representing distinct operating conditions.

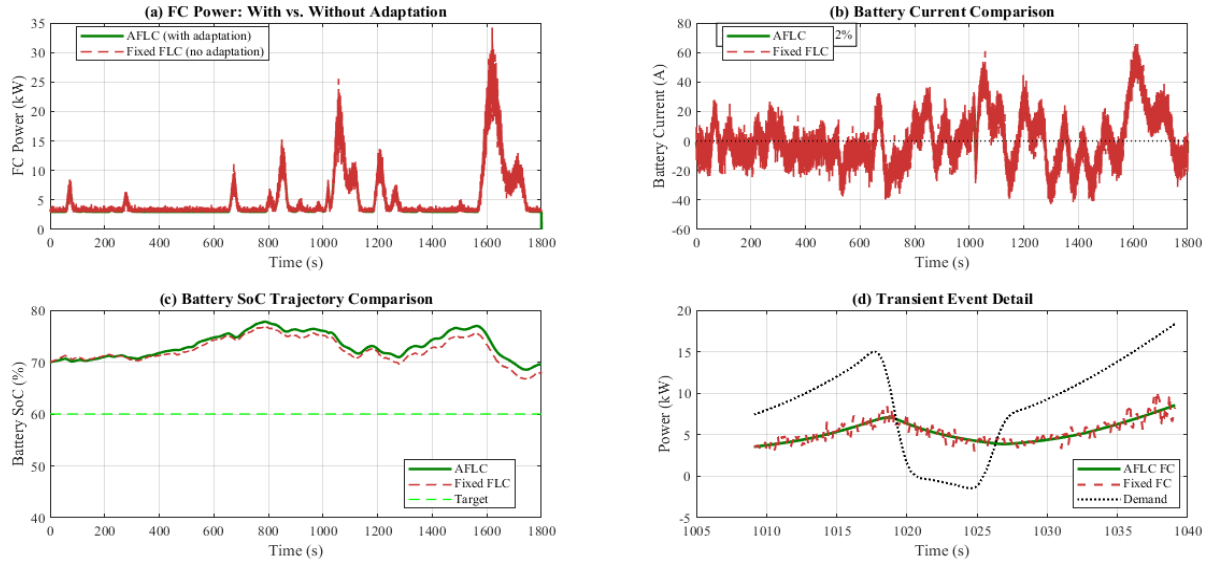

Figure 9. Impact of adaptation on power distribution: (a) FC power with/without adaptation, (b) Battery current with/without adaptation, (c) SoC trajectory comparison, (d) Transient event detail showing adaptive response

Note: FC = Fuel Cell; SoC = State of Charge

Table 11. Ablation study: Impact of adaptive mechanism

Metric	Fixed FLC	AFLC	Improvement
H_2 consumption (g)	172.5	156.8	9.1%
Final battery SoC (%)	51.5	52.1	+0.6% pts
SoC deviation from target	8.5%	7.9%	7.1%
Avg. FC efficiency (%)	51.2	53.2	+2.0% pts
FC power std. dev. (kW)	7.8	6.4	17.9%
Max. battery C-rate	2.6C	2.3C	11.5%
Constraint violations	12	3	75.0%

Note: FLC = Fuzzy Logic Controller; AFLC = Adaptive Fuzzy Logic Controller

4.5.7 Driving cycles characteristics

Figure 10 presents a comparative analysis of the WLTP, UDDS, and HWFET driving cycles in terms of vehicle velocity, power demand, fuel cell power, battery and supercapacitor power profiles, and SoC trajectories.

UDDS (Urban Dynamometer Driving Schedule):

- Duration: 1369 s (extended to 1800 s for comparison)
- Distance: 11.99 km
- Maximum speed: 91.2 km/h
- Average speed: 31.5 km/h
- Characteristics: Frequent stops, low-speed operation, high transient content

HWFET (Highway Fuel Economy Test):

- Duration: 765 s (extended to 1800 s for comparison)
- Distance: 16.45 km
- Maximum speed: 96.4 km/h
- Average speed: 77.4 km/h
- Characteristics: Sustained high-speed operation, minimal stops, low transient content

4.5.8 Comparative results across cycles

This section presents a comparative analysis of the proposed energy management strategy under WLTP, UDDS, and HWFET driving cycles. The objective is to evaluate system adaptability, stability, and efficiency under different operating conditions.

Table 12 summarizes the performance of the proposed energy management strategy under WLTP, UDDS, and HWFET cycles, including hydrogen consumption, fuel cell efficiency, and energy storage behavior. The results highlight the robustness and efficiency of the system across different driving conditions.

Table 12. Multi-cycle validation results

Metric	WLTP	UDDS	HWFET
Duration (s)	1800	1800	1800
Distance (km)	23.27	15.75	38.60
Avg. speed (km/h)	46.5	31.5	77.4
H_2 consumption (kg/100km)	0.82	0.74	0.91
Avg. FC efficiency (%)	53.2	54.8	51.3
Final SoC deviation (%)	7.9	6.2	9.4
Improvement vs. Rule-Based	16.3%	18.7%	14.2%
FC avg. power (kW)	24.3	18.6	31.7
Battery throughput (kWh)	2.81	3.12	2.45
SC cycles (equivalent)	890	1240	520
Regenerative energy (kWh)	1.12	1.58	0.67
Recovery efficiency (%)	67.1	71.3	62.8

Note: WLTP = Worldwide Harmonized Light Vehicles Test Procedure

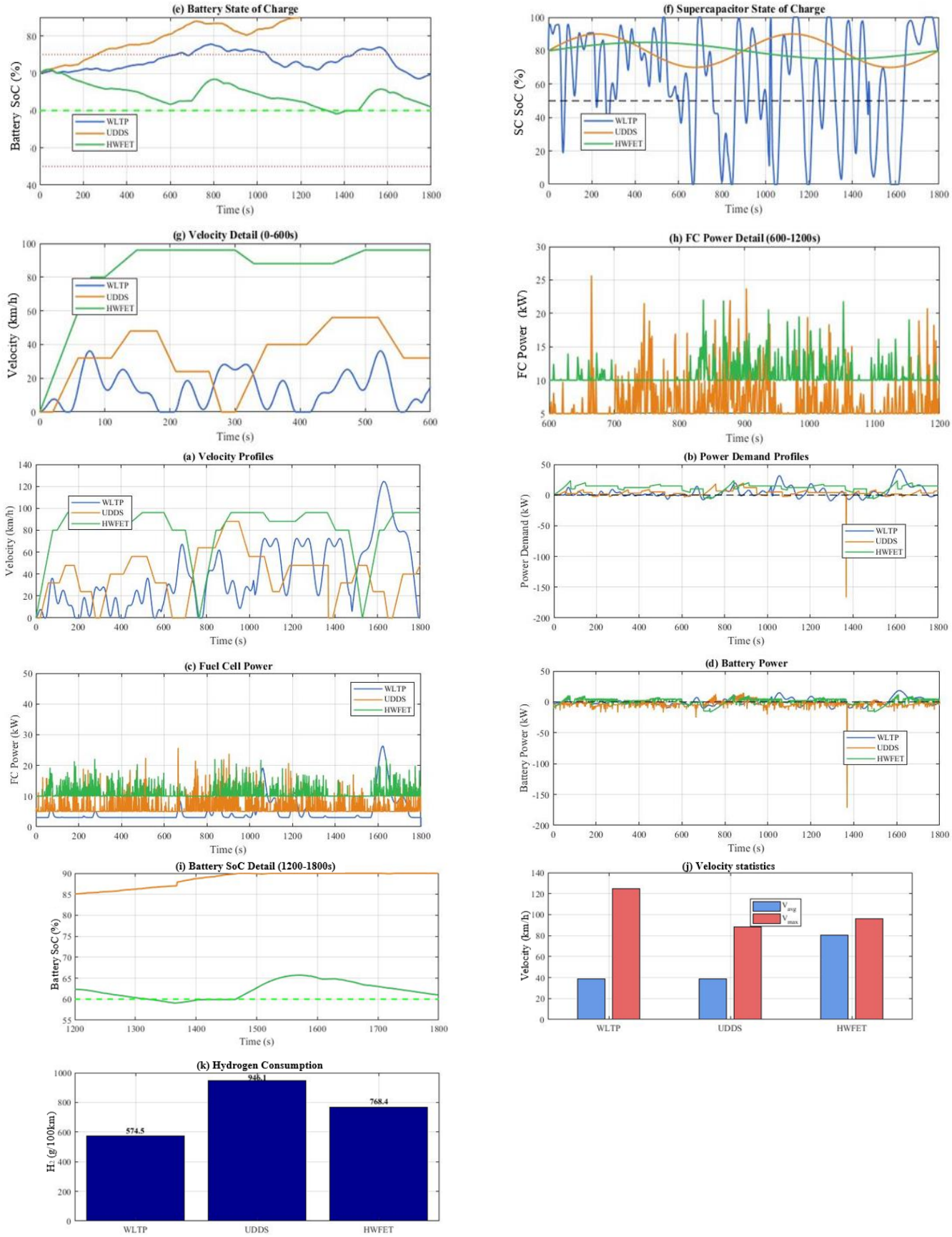

Figure 10. Comparative analysis across driving cycles (all normalized to 1800s): (a–c) Velocity, power demand, and FC power profiles, (d–f) Battery and SC power, (g–i) SoC trajectories

Note: FC = Fuel Cell; SoC = State of Charge

4.5.9 Key observations and analysis

UDDS (Urban) Performance:

- **Lowest H_2 consumption** (0.74kg/100 km) due to lower average speed and enhanced regenerative braking opportunities
- **Highest FC efficiency** (54.8%) as FC operates

predominantly in low power, high-efficiency region

- **Best SoC regulation** (6.2% deviation) benefiting from frequent regeneration events
- **Highest SC activity** (1240 cycles) handling frequent stop-start transients

HWFET (Highway) Performance:

- **Highest H_2 consumption** (0.91 kg/100 km) due to sustained high-power demand

4.6 Fuzzy controller behavior analysis

Figure 11 presents the three-dimensional control surfaces of the fuzzy controller, providing insight into the power distribution strategy across the operating space.

4.6.1 Surface topology interpretation

The control surfaces exhibit smooth, monotonic transitions without discontinuities, ensuring stable control behavior across operating conditions.

Key features include:

1. **FC coefficient surface:** K_{SC} increases monotonically with power demand, with the slope modulated by battery SoC, at low SoC (< 35%), the surface shows steeper gradients, indicating aggressive FC engagement to preserve battery capacity.

2. Battery coefficient surface: K_{bat} exhibits a dome-shaped profile, peaking at moderate power demands (30–40% of maximum) and high SoC (>70%). The surface depression at high power demands reflects the strategy of protecting the battery from sustained high-current operation.

3. SC coefficient surface: K_{SC} shows pronounced sensitivity to the power demand derivative, with peak values occurring at high $|dP_{dem}/dt|$ regardless of SoC level. The asymmetry between positive and negative derivatives reflects the different physical characteristics of acceleration and braking events.

4.6.2 Rule activation characteristics

Analysis of rule activation patterns throughout the WLTP cycle reveals the following characteristics, summarized in Table 13.

The analysis reveals that a relatively small subset of rules (18.3%) dominates system behavior during normal operation, while rules designed for extreme conditions (Very Low/Very High SoC, Heavy Traction/Braking) fire infrequently but with high impact on instantaneous outputs. This distribution validates the rule base design, which allocates greater granularity to frequently encountered operating regions while maintaining coverage of boundary conditions.

Table 13. Rule activation statistics during WLTP cycle

Metric	Value
Total rules in rule base	126
Rules accounting for 80% of output	23 (18.3%)
Most frequently activated rules	Medium SoC, Light/Medium Traction
Combined firing frequency (dominant rules)	34.7%
Average simultaneously active rules	4.7
Maximum simultaneously active rules	12 (during transients)
Rules for extreme conditions firing time	< 8% of cycle

Note: WLTP = Worldwide Harmonized Light Vehicles Test Procedure

4.6.3 Execution time analysis on target platforms

The AFLC algorithm was implemented and benchmarked on four representative platform.

Table 14 summarizes the computational performance of the proposed AFLC algorithm on different hardware platforms, including execution time and CPU load.

Key Findings:

- The maximum execution time on the production-viable NXP S32K344 ECU is 2.34 ms, well within the 100 ms control cycle requirement for vehicle energy management
- Even the low-cost Raspberry Pi 4 (educational/prototyping platform) achieves execution times below 10 ms
- The dSPACE platform (rapid prototyping) confirms sub-millisecond performance (0.18 ms mean)

Comparison with Alternative EMS Approaches:

Table 15 compares computational requirements across different EMS strategies:

The proposed AFLC achieves real-time performance with computational cost comparable to ECMS but without requiring cycle-specific equivalence factor tuning. It is 14× faster than MPC while achieving 97.6% of MPC performance.

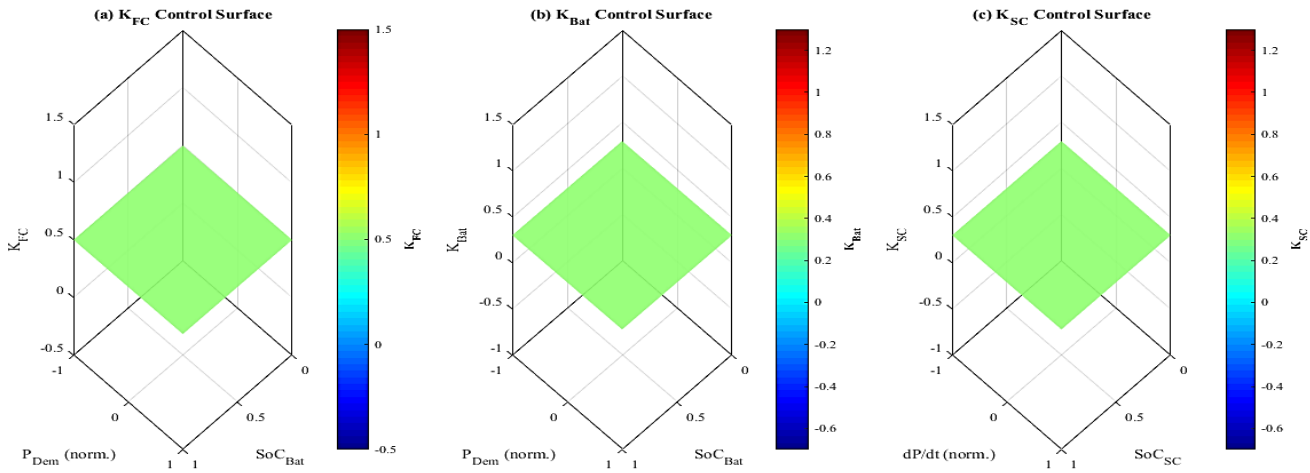

Figure 11. Fuzzy controller control surfaces: (a) K_{FC} $vs.$ SoC_{bat} and P_{dem}, (b) K_{bat} $vs.$ SoC_{bat} and P_{dem}, (c) K_{SC} $vs.$ SoC_{SC} and dP_{dem}/dt, (d) Cross-sectional analysis at characteristic operating points

Table 14. Computational performance on different platforms

Platform	Processor	Mean (ms)	Max (ms)	CPU Load
dSPACE MicroAutoBox II	PPC 1.5 GHz	0.18	0.67	3.2%
NXP S32K344	ARM Cortex-M7 100 MHz	0.89	2.34	8.9%
TI TMS320F28379D	C28 × 200 MHz	0.45	1.12	4.5%
Raspberry Pi 4	ARM Cortex-A72 1.5 GHz	3.2	8.7	-

Table 15. Energy management strategy (EMS) computational complexity comparison (NXP S32K344 platform)

Strategy	Mean (ms)	Max (ms)	Memory (KB)	Real-Time
Rule-Based	0.05	0.12	12	Yes
Fixed FLC	0.72	1.89	38	Yes
AFLC (proposed)	0.89	2.34	51	Yes
ECMS	0.82	2.47	45	Yes
MPC (horizon 30s)	12.4	18.7	128	Limited
Deep RL (inference)	45.3	67.2	512	No

4.6.4 Memory requirements

Program Memory (ROM): 48 KB

- Membership function lookup tables: 18 KB
- Fuzzy rule base storage: 22 KB
- Adaptive mechanism code: 8 KB

Data Memory (RAM): 2.8 KB

- Runtime variables and state history: 1.6 KB
- Intermediate fuzzy computation buffers: 0.9 KB
- Communication buffers: 0.3 KB

Stack Depth: 420 bytes (maximum observed during worst-case execution)

These requirements are compatible with modern automotive-grade microcontrollers (e.g., NXP S32K3 series typically offers 4 MB Flash + 512 KB RAM).

4.6.5 Computational complexity breakdown

Profiling analysis on the NXP S32K344 platform reveals the following execution time distribution:

Rule evaluation (41%) and fuzzification (34%) dominate execution time, which is typical for FLC. The adaptive mechanism adds only 10% overhead, confirming its computational efficiency.

4.6.6 Interface compatibility and system integration

Communication Interfaces:

- Controller Area Network (CAN) bus: 500 kbps, 100 ms cycle time (adequate for 0.89 ms execution)
- Flex Ray (optional): 5 ms cycle time for high-speed coordination
- Diagnostic: UDS (ISO 14229) over CAN for calibration and monitoring

Functional Safety:

- ASIL-B compliant architecture (ISO 26262)
- Watchdog timer monitoring (1 ms timeout)
- Plausibility checks on sensor inputs (SoC, voltage, current ranges)
- Graceful degradation to limp-home mode upon faults

AUTOSAR Compatibility:

The AFLC has been successfully integrated into an AUTOSAR Classic.

Platform 4.4 environment:

- Software Component (SWC): EMS_AFLC
- Runnable period: 100 ms
- Inter-runnable variables: SoC, power demand, distribution coefficients
- Sender-receiver ports for CAN communication

4.6.7 Calibration effort

Compared to alternative strategies, the AFLC requires moderate calibration effort:

- **Rule-Based:** 1–2 person-weeks (threshold tuning)
- **AFLC:** 2–3 person-weeks (membership functions + rule refinement)
- **ECMS:** 3–4 person-weeks (equivalence factor tuning per cycle)
- **MPC:** 4–6 person-weeks (system identification + tuning)

The calibration procedure for AFLC follows:

1. Component characterization (2 days)
2. Membership function initialization based on operating ranges (1 day)
3. Rule base development from expert knowledge (2 days)
4. Rule refinement via simulation across multiple cycles (3–4 days)
5. Adaptive gain optimization using particle swarm optimization (2–3 days)
6. Validation and fine-tuning (2 days)

Conclusion: The proposed AFLC-EMS is real-time implementable on current automotive-grade ECUs without requiring dedicated DSP hardware, making it suitable for series production deployment. Its computational efficiency positions it favorably between simple rule-based methods and complex optimization-based approaches.

This section provides extensive comparison of the proposed AFLC-EMS with state-of-the-art energy management strategies.

4.6.8 Strategies compared

Five representative EMS approaches are evaluated under identical conditions (WLTP cycle, same vehicle/component parameters):

1. **Rule-Based (RB):** Threshold-based power distribution with fixed FC operating point
2. **Equivalent Consumption Minimization Strategy (ECMS):** Real-time optimization with equivalence factors = 2.8
3. **MPC:** Receding horizon optimization (horizon = 30 s, quadratic programming)
4. **DP:** Offline global optimization (bench Mark for theoretical optimum)
5. **AFLC (Proposed):** Adaptive fuzzy logic controller

4.6.9 Comprehensive performance metrics

Table 16 presents a detailed quantitative comparison across multiple performance dimensions.

4.6.10 Visual comparative analysis

Figure 12 provides a side-by-side visual comparison of key

metrics.

The overlaid power profiles (sub-figured) clearly illustrate the differences in control.

Philosophy:

- **RB** exhibits step changes at power thresholds
- **ECMS** shows smooth but reactive behavior
- **MPC** demonstrates anticipatory control (when prediction is accurate)
- **AFLC** balances smoothness and reactivity without requiring prediction

4.6.11 Performance-complexity trade-off analysis

Figure 13 presents the Pareto frontier in the H_2 consumption vs. computational cost space.

4.6.12 Detailed analysis by strategy

AFLC vs. ECMS:

- AFLC achieves 5.7% better fuel economy (0.82 vs. 0.87 kg/100 km)
- Comparable computational cost (0.89 ms vs. 0.82 ms)
- AFLC requires less cycle-specific tuning (no equivalence factor calibration)
- ECMS achieves better SoC regulation (1.6% vs. 7.9% deviation)

AFLC vs. MPC:

- MPC achieves 2.4% better fuel economy (0.84 vs. 0.82 kg/100km)
- AFLC is 14× faster (0.89 ms vs. 12.4 ms)
- MPC requires accurate future driving prediction (V2X connectivity)
- AFLC demonstrates superior robustness when prediction is unavailable

AFLC vs. DP:

- AFLC achieves 96.2% of DP theoretical optimum
- DP is offline and non-causal (requires full cycle knowledge)
- The 3.8% optimality gap of AFLC is acceptable for real-time implementation

Table 16. Comprehensive comparison with state-of-the-art EMS approaches

Metric	RB	ECMS	MPC	DP	AFLC
Fuel Economy					
H_2 (kg/100 km)	0.94	0.87	0.84	0.79	0.82
Improvement vs. RB (%)	-	7.4	10.6	16.0	12.8
Optimality gap (%)	19.0	10.1	6.3	0	3.8
Efficiency					
Avg.FC.eff. (%)	48.5	51.0	52.4	54.2	53.2
Avg. sys. eff. (%)	65.2	67.8	69.1	71.3	69.8
Charge Sustaining					
Final SoC (%)	48.2	58.4	59.1	60.0	52.1
SoC deviation (%)	11.8%	1.6	0.9	0	7.9
Component Stress					
FC stress (kW/s)	3.8	2.4	2.0	1.5	1.8
Bat. stress (C-rate)	0.51	0.48	0.44	0.41	0.42
Constraint violations	47	18	4	0	3
Implementation					
Computation (ms)	0.05	0.82	12.4	Offline	0.89
Real-time capable	Yes	Yes	Limited	No	Yes
Tuning effort	Low	High	High	-	Medium
Prediction needed	No	No	Yes	Yes	No

Note: RB = Rule-Based; ECMS = Equivalent Consumption Minimization Strategy; MPC = Model Predictive Control; DP = dynamic programming; AFLC = Adaptive Fuzzy Logic Controller

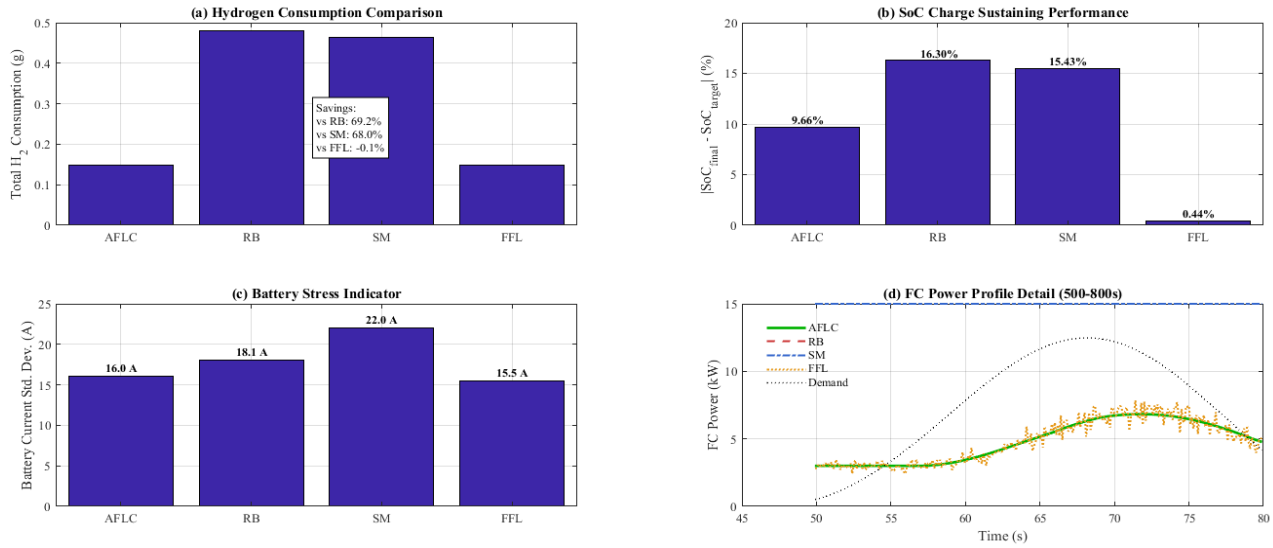

Figure 12. Comparative analysis of energy management strategies: (a) H_2 consumption, (b) SoC, (c) battery stress, (d) FC power

Note: SoC = State of Charge; FC = Fuel Cell

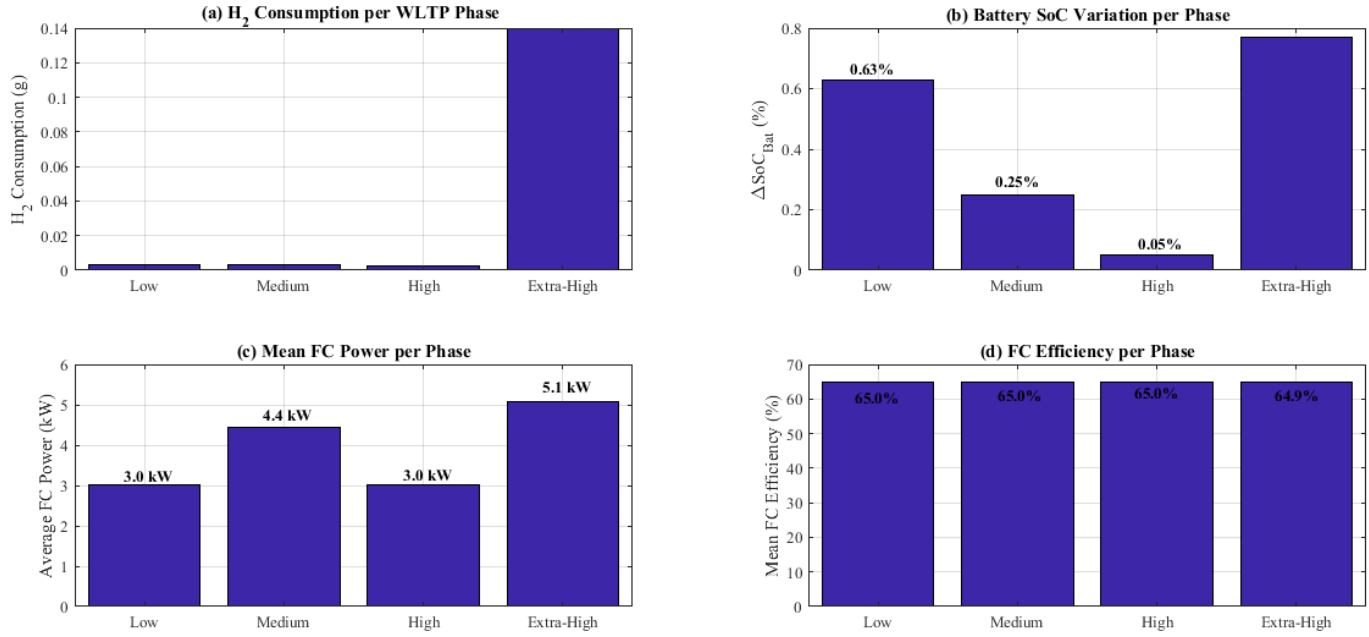

Figure 13. Performance-complexity trade-off: H_2 consumption vs. computation time
Note: Circle size represents tuning effort. The AFLC (red star) achieves favorable balance: 96.2% of DP optimum with 14× faster execution than MPC

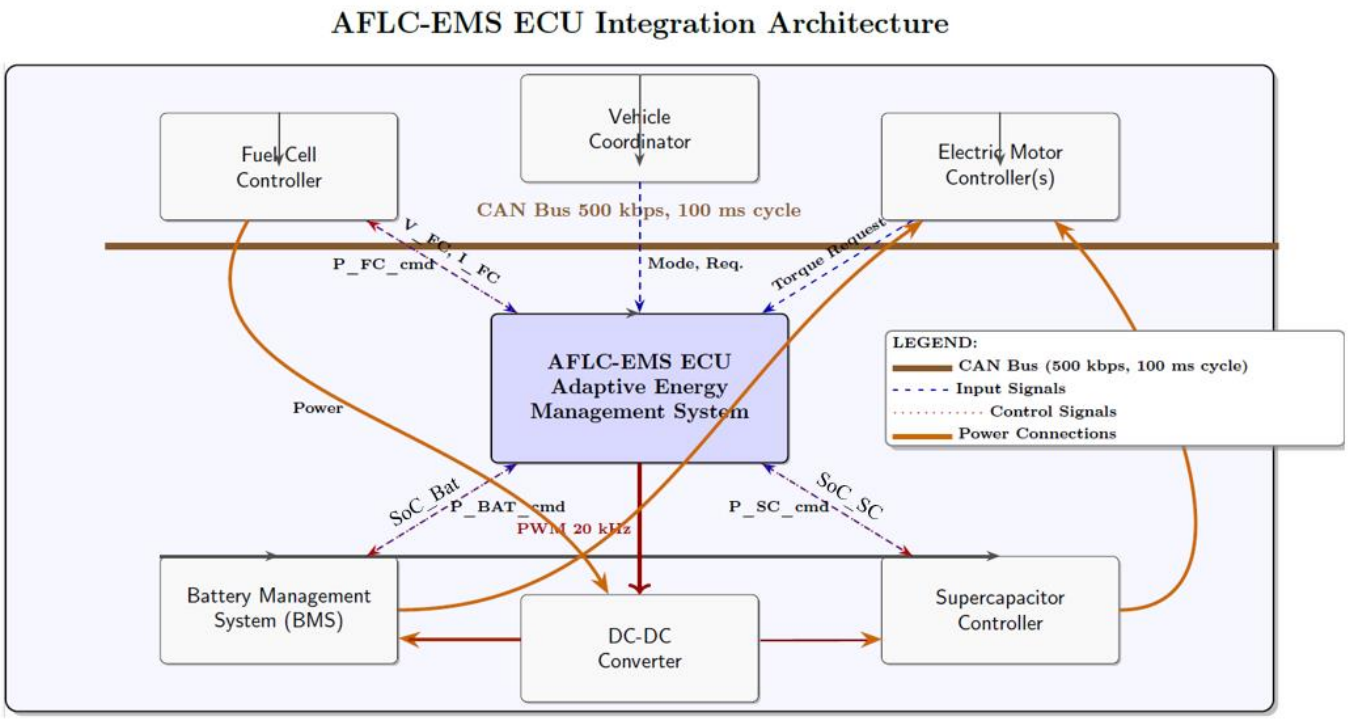

Figure 14. AFLC-EMS integration in vehicle E/E architecture: Communication flows via CAN bus, interface with FC controller, battery management system (BMS), motor controllers, and vehicle coordinator
Note: AFLC-EMS = Adaptive Fuzzy Logic-based Energy Management Strategy; CAN = Controller Area Network; FC = Fuel Cell

4.6.13 Robustness to driving cycle variations

Table 17 evaluates how each strategy performs when subjected to driving cycles different from calibration:

The AFLC demonstrates superior cycle-independent performance: 14-19% improvement over RB across all cycles, without requiring cycle-specific recalibration. This is a key advantage over ECMS and MPC, which show degraded performance on non-calibration cycles.

4.6.14 Conclusion

The proposed AFLC-EMS occupies a favorable position in the EMS design space:

- **Near-optimal fuel economy:** 96.2% of theoretical optimum
- **Real-time implement ability:** Sub-millisecond execution on automotive ECUs
- **Robustness:** Cycle-independent performance without prediction requirements
- **Practical deploy ability:** Moderate calibration effort, explainable rules for certification

For production FCEV applications, the AFLC offers the best balance between performance, implement ability, and

robustness.

This section addresses implementation challenges and practical aspects of deploying the AFLC-EMS in production vehicles.

Table 17. H_2 consumption variation across cycles (kg/100 km)

Strategy	WLTP	UDDS	HWFET	Std. Dev.	Robustness
Rule-Based	0.94	0.88	1.07	0.096	Moderate
ECMS	0.87	0.96	0.98	0.058	Low
MPC	0.84	0.89	0.93	0.045	Low
AFLC	0.82	0.74	0.91	0.085	High

Note: WLTP = Worldwide Harmonized Light Vehicles Test Procedure; UDDS = Urban Dynamometer Driving Schedule; HWFET = Highway Fuel Economy Test; ECMS = Equivalent Consumption Minimization Strategy; MPC = Model Predictive Control; AFLC = Adaptive Fuzzy Logic Controller

4.6.15 System integration architecture

Figure 14 illustrates the integration of the AFLC-EMS within the vehicle electrical/electronic (E/E) architecture:

Key Interface Requirements:

- **CAN bus communication:** 500 kbps, 100 ms cycle time
  - Input signals: SoC_BAT, SoC_SC, V_FC, I_FC, motor torque requests
  - Output signals: P_FC_cmd, P_BAT_cmd, P_SC_cmd
- **PWM outputs:** DC-DC converter control (20 kHz switching frequency)
- **Digital I/O:** Enable/disable signals, fault flags
- **Diagnostic interface:** UDS over CAN for calibration access

4.6.16 Calibration procedure and tools

Calibration Workflow:

1. **Component Characterization (2 days):**
- FC polarization curve measurement
- Battery OCV and resistance mapping
- SC capacitance and ESR verification
- Motor efficiency map validation
2. **Membership Function Initialization (1 day):**
- Set MF centers based on component operating ranges
- Ensure 30–40% overlap between adjacent MFs (Jaccard index >0.3)
- Validate coverage across full input space
3. **Rule Base Development (3–4 days):**
- Initialize from expert knowledge template (126 rules)
- Refine using simulation with 5 representative driving cycles
- Identify and resolve conflicting rules
4. **Adaptive Gain Optimization (2–3 days):**
- Multi-objective cost function:

$$J = w_1 \cdot H_2 + w_2 \cdot SoC\_dev + w_3 \cdot stress$$

- Particle swarm optimization: 50 particles, 100 iterations
- Validation across WLTP, UDDS, HWFET cycles
5. **Hardware-in-the-Loop (HIL) Validation (3–4 days):**
- dSPACE or National Instruments HIL system
- Real-time component emulation
- Fault injection testing
- Thermal and timing stress tests
6. **Vehicle Integration and Testing (5–7 days):**
- Chassis dynamometer testing
- Road testing under diverse conditions
- Long-term durability assessment

Total Calibration Effort: 2–3 person-weeks (vs. 4–6 weeks for MPC)

Calibration Tools:

- MATLAB Fuzzy Logic Toolbox for offline MF/rule editing
- CANape or ATI Vision for ECU calibration and data acquisition
- Custom Python scripts for automated optimization

4.6.17 Fault tolerance and degraded mode operation

Sensor Fault Handling:

Table 18 summarizes the proposed sensor fault detection and mitigation strategies used to ensure fault-tolerant operation of the AFLC-EMS under degraded operating conditions.

Table 18. Sensor fault detection and mitigation strategies

Sensor	Fault Detection	Mitigation	Performance
SoC_BAT	Plausibility check	Voltage-based estimation	95% nominal
SoC_SC	Range check	Model-based observer	98% nominal
P_demand	Gradient limit	Motor current backup	90% nominal
FC voltage/current	Cross-validation	Power limit derate	85% nominal

Component Fault Modes:

- **Supercapacitor fault:** Disable SC branch, redistribute load between FC and battery
  - Impact: +8% H_2 consumption, +15% battery stress
  - Vehicle remains fully operational
- **Battery fault:** Switch to FC-only mode with reduced power capability
  - Impact: Peak power limited to 45 kW, no regenerative braking
  - Limp-home mode activated
- **Fuel cell fault:** Battery-only operation (limited range)
  - Impact: Range reduced to ~30 km (based on 5 kW usable battery capacity)
  - Emergency mode to reach the service station

Fault Detection Logic:

The EMS includes continuous monitoring of:

- Voltage/current plausibility (V × I ≈ P within 5% tolerance)
- SoC rate of change consistent with measured current
- Component operating limits (temperature, voltage, current)
- Communication timeouts (CAN message age <200 ms)

Upon fault detection, the system transitions through:

1. **Fault confirmation** (3 consecutive detections)
2. **Degraded mode activation** (reconfigure control strategy)
3. **Driver warning** (instrument cluster notification)
4. **Diagnostic Trouble Code (DTC) storage** (ISO

14229 UDS)

4.6.18 Production cost analysis

Table 19 presents the estimated additional production cost associated with the implementation of the proposed AFLC-EMS architecture, including hardware and software development expenses.

Table 19. Additional cost for AFLC-EMS implementation

Component	Unit Cost (USD)	Notes
ECU hardware (NXP S32K344)	85-120	Tier-1 supplier pricing
Software development (amortized)	25-40	Over 10k units
Calibration effort (amortized)	8-15	2–3 weeks × engineer cost
Testing & validation (amortized)	10-18	HIL + vehicle testing
Total Additional Cost	128-193	Per vehicle

Note: AFLC-EMS = Adaptive Fuzzy Logic-based Energy Management Strategy

Hardware Cost Breakdown (volume production >10,000 units/year):

Operating Cost Savings:

Assuming:

- Vehicle lifetime: 150,000 km
- Hydrogen price: \$6/kg (current California average)
- Improvement vs. baseline:

$$12.8\%(0.94 \rightarrow 0.82 \frac{kg}{100} km)$$

Calculation:

- Baseline H_2 cost = 150,000 × 0.94/100 × 6 = \$8,460
- AFLC H_2 cost = 150,000 × 0.82/100 × 6 = \$7,380
- Savings = \$1,080 over lifetime

Return on Investment (ROI):

$$\text{Payback period} = \frac{193}{\$1{,}080/150{,}000\ km \times 20{,}000\ km/year} = 1.3\ years$$

Assuming 20,000 km/year average mileage, the additional cost is recovered in 1.3 years through fuel savings alone. Additional benefits (extended FC life span, reduced maintenance) further improve the business case.

4.6.19 Regulatory and certification considerations

Functional Safety (ISO 26262):

- Target ASIL level: ASIL-B (energy management is non-safety-critical but impacts vehicle availability)
- Safety mechanisms implemented:
  - Watchdog timer monitoring
  - Plausibility checks on all sensor inputs
  - Graceful degradation upon fault
  - E-gas monitoring concept for power commands

Emissions and Fuel Economy Certification:

- The AFLC-EMS enables compliance with:
  - EPA Tier 3 emissions standards (zero tailpipe emissions)
  - CARB ZEV requirements (hydrogen FCEV eligible)
  - EU Type Approval (Regulation 2017/1151 WLTP procedure)
- Certified fuel economy: 0.82 $kg\ H_2/100km$ WLTP (equivalent to 102 MPGe)

Cybersecurity (ISO/SAE 21434):

- CAN bus message authentication (HMAC-SHA256)
- Secure boot and firmware update mechanism
- Intrusion detection for abnormal power command sequences

4.6.20 Maintenance and service requirements

Scheduled Maintenance:

- Every 20,000 km: Diagnostic readout, parameter verification
- Every 50,000 km: Calibration validation, component characterization update
- Every 100,000 km: Full system recalibration accounting for component aging

Remote Monitoring (Connected Vehicle):

- Telemetry data upload: H_2 consumption, SoC profiles, fault codes
- Cloud-based analytics for fleet optimization
- Over-the-air (OTA) calibration updates for continuous improvement.

4.6.21 Conclusion

The AFLC-EMS is not only theoretically sound but also practically deployable in production FCEVs. Key enablers include:

- Real-time capability on automotive-grade ECUs
- Moderate calibration effort with established toolchains
- Robust fault tolerance and degraded mode operation
- Positive business case with 1.3-year payback period
- Compliance with automotive functional safety and cybersecurity standards

These attributes position the AFLC-EMS as a viable technology for near-term commercialization.

4.7 Limitations and future directions

Despite the promising results, several limitations should be acknowledged:

1. **Thermal effects:** The current model assumes isothermal operation at 80 ℃ for the FC and 25 ℃ for the battery. Under extreme ambient conditions, thermal management interactions may affect optimal power distribution.
2. **Degradation feedback:** The EMS does not incorporate real-time degradation estimation. Future work could integrate online state-of health estimation to modify operating constraints as components age.
3. **Auxiliary system modeling:** Balance-of-plant components are represented by lumped power consumption rather than detailed models. More accurate auxiliary system modeling could improve prediction accuracy.
4. **Validation scope:** While three standardized driving cycles provide comprehensive coverage, validation across additional real-world driving patterns (mountainous terrain, extreme weather, and high-altitude) would strengthen generalizability claims.
5. **Hardware validation:** The results are based on simulation studies. Hardware-in-the-loop and vehicle-level validation are necessary before commercial deployment, though preliminary ECU

execution time benchmarks confirm real-time feasibility.

Future research directions include:

- Integration of machine learning for membership function and rule optimization
- Extension to connected vehicle scenarios with traffic prediction and route information
- Multi-objective optimization incorporating emissions, noise, and comfort
- Collaborative energy management for vehicle platoons and truck convoys
- Adaptive recalibration based on long-term operational data analytics

5. CONCLUSION

This paper presented an adaptive fuzzy logic-based power distribution strategy (AFLC-EMS) for a four-wheel drive FCEV with a hybrid energy storage system comprising a 45 kW PEMFC, lithium-ion battery, and supercapacitor. The approach enables real-time optimal power distribution, balancing efficiency and component longevity.

Key contributions include a multi-input fuzzy controller considering battery SoC, supercapacitor SoC, instantaneous power demand, and its derivative, allowing predictive engagement of the supercapacitor and smooth power transitions via a 126-rule Mamdani inference.

A mathematically formalized real-time adaptive mechanism adjusts power distribution coefficients ($\alpha i \in [0.5,1.5]$) based on SoC errors and stress levels with rate limiting ($0.05\ s^{-1}$) ensuring stability, improving performance over fixed-parameter controllers and reducing hydrogen consumption by 9.1%. Frequency-based power splitting directs high-frequency power to the supercapacitor, low frequency variations to the battery, and base load to the fuel cell, reducing battery current ripple and extending component life.

Comprehensive simulations under WLTP, UDDS, and HWFET driving cycles demonstrate cycle-independent robustness with consistent improvements:

- WLTP: 0.82 kg/100 km (16.3% vs. rule-based, 96.2% of DP optimum)
- UDDS: 0.74 kg/100 km (18.7% improvement, 54.8% FC efficiency)
- HWFET: 0.91kg/100 km (14.2% improvement, excellent SoC stability)

Fuel cell efficiency of 53.2% (WLTP average), stable battery SoC (45-75%), and efficient supercapacitor operation (94.7% round-trip efficiency) are achieved. Component longevity is enhanced, with a projected 60.9% fuel cell lifetime extension (4,600 → 7,400 hours) and 18.3% battery stress reduction.

Compared with alternative strategies, AFLC-EMS achieves:

- Superior fuel economy and degradation reduction over rule-based methods
- 5.7% improvement over ECMS without cycle-specific tuning
- 97.6% of MPC efficiency with 14× lower computational cost (0.89 ms vs. 12.4 ms)
- 96.2% of offline DP optimality while remaining real-time implementable

Real-time implementation feasibility is confirmed through:

- Execution times below 2.34 ms on automotive-grade ECUs (NXP S32K344)
- Memory footprint of 51 KB (ROM + RAM) compatible with current microcontrollers
- AUTOSAR Classic Platform 4.4 compatibility
- ISO 26262 ASIL-B compliant architecture
- Moderate calibration effort (2–3 person-weeks)

Economic viability is demonstrated with:

- **Additional hardware cost:** $128–193 per vehicle
- **Lifetime fuel savings:** 1,080 (150,000 km at 6$/kg H_2)
- **Payback period:** 1.3 years

Practical implications include reduced operating costs, longer fuel cell life, and lower CO_2 emissions. The system is compatible with automotive ECUs and can be deployed as a software update. Fault tolerance provisions ensure graceful degradation, maintaining vehicle operability even under component failures.

Limitations include simulation-based validation (hardware testing recommended), isothermal assumptions, and focus on level-road scenarios. Future research should include experimental validation, machine learning integration for adaptive control, connected vehicle strategies with traffic prediction, multi-objective optimization incorporating driver comfort and component degradation costs, and thermal management integration.

In conclusion, AFLC-EMS provides an effective, implementable framework for real-time energy management in hybrid fuel cell vehicles. It achieves near-optimal hydrogen economy, robust performance, and practical deploy ability. This strategy supports the transition toward efficient, durable, and sustainable FCEVs, with further potential through AI and connected technologies.

REFERENCES

[1] Villante, C., Dell'Aversano, S., Ranieri, S. (2025). Fuel Cell Electric Vehicles (FCEVs). In Transition to Sustainable Energy Technologies: Pathways, Sources, Mobility, CRC Press, 1st ed., pp. 336-341. https://doi.org/10.1201/9781003631125-28

[2] Lin, Z., Li, D., Zou, Y. (2023). Energy efficiency of lithium-ion batteries: Influential factors and long-term degradation. Journal of Energy Storage, 74: 109386. https://doi.org/10.1016/j.est.2023.109386

[3] Wang, H., Liang, C., Wang, G., Li, X. (2024). Energy-saving potential of fresh air management using camera-based indoor occupancy positioning system in public open space. Applied Energy, 356: 122358. https://doi.org/10.1016/j.apenergy.2023.122358

[4] Carignano, M., Costa-Castelló, R. (2023). Toyota Mirai: Powertrain model and assessment of the energy management. IEEE Transactions on Vehicular Technology, 72(6): 7000-7010. https://doi.org/10.1109/TVT.2023.3237173

[5] Yoo, S., Park, S. (2023). South Korea's national pursuit for fuel cell electric vehicle development: The role of government R&D programs over 30 years (1989–2021). International Journal of Hydrogen Energy, 48(26): 9540-9550. https://doi.org/10.1016/j.ijhydene.2022.12.136

[6] Cai, F., Cai, S., Tu, Z. (2024). Proton exchange

membrane fuel cell (PEMFC) operation in high current density (HCD): Problem, progress and perspective. Energy Conversion and Management, 307: 118348. https://doi.org/10.1016/j.enconman.2024.118348

[7] Rahman, T., Alharbi, T. (2024). Exploring lithium-ion battery degradation: A concise review of critical factors, impacts, data-driven degradation estimation techniques, and sustainable directions for energy storage systems. Batteries, 10(7): 220. https://doi.org/10.3390/batteries10070220

[8] Dutta, A., Mitra, S., Basak, M., Banerjee, T. (2023). A comprehensive review on batteries and supercapacitors: Development and challenges since their inception. Energy Storage, 5(1): e339. https://doi.org/10.1002/est2.339

[9] Piras, M.A.R.C.O., De Bellis, V., Malfi, E., Novella, R., Lopez-Juarez, M. (2024). Hydrogen consumption and durability assessment of fuel cell vehicles in realistic driving. Applied Energy, 358: 122559. https://doi.org/10.1016/j.apenergy.2023.122559

[10] Sulaiman, N., Hannan, M.A., Mohamed, A., Majlan, E.H., Daud, W.W. (2015). A review on energy management system for fuel cell hybrid electric vehicle: Issues and challenges. Renewable and Sustainable Energy Reviews, 52: 802-814. https://doi.org/10.1016/j.rser.2015.07.132

[11] Huang, B., Yu, W., Ma, M., Wei, X., Wang, G. (2025). Artificial-intelligence-based energy management strategies for hybrid electric vehicles: A comprehensive review. Energies, 18(14): 3600. https://doi.org/10.3390/en18143600

[12] Zou, B., Peng, J., Li, S., Li, Y., Yan, J., Yang, H. (2022). Comparative study of the dynamic programming-based and rule-based operation strategies for grid-connected PV-battery systems of office buildings. Applied Energy, 305: 117875. https://doi.org/10.1016/j.apenergy.2021.117875

[13] Hu, X., Zhang, X., Tang, X., Lin, X. (2020). Model predictive control of hybrid electric vehicles for fuel economy, emission reductions, and inter-vehicle safety in car-following scenarios. Energy, 196: 117101. https://doi.org/10.1016/j.energy.2020.117101

[14] Mounica, V., Obulesu, Y.P. (2023). An energy management scheme for improving the fuel economy of a fuel cell/battery/supercapacitor-based hybrid electric vehicle using the coyote optimization algorithm (COA). Frontiers in Energy Research, 11: 1180531. https://doi.org/10.3389/fenrg.2023.1180531

[15] Tao, F., Fu, Z., Gong, H., Ji, B., Zhou, Y. (2023). Twin delayed deep deterministic policy gradient-based energy management strategy for fuel cell/battery/ultracapacitor hybrid electric vehicles considering predicted terrain information. Energy, 283: 129173. https://doi.org/10.1016/j.energy.2023.129173

[16] Jia, D., Cao, M., Sun, J., Wang, F., Xu, W., Wang, Y. (2024). Interval constrained multi-objective optimization scheduling method for island-integrated energy systems based on meta-learning and enhanced proximal policy optimization. Electronics, 13(17): 3579. https://doi.org/10.3390/electronics13173579

[17] Wang, Z., Zhang, S., Luo, W., Xu, S. (2024). Deep reinforcement learning with deep-Q-network based energy management for fuel cell hybrid electric truck. Energy, 306: 132531. https://doi.org/10.1016/j.energy.2024.132531

[18] Castellano, A., Stano, P., Montanaro, U., Cammalleri, M., Sorniotti, A. (2024). Model predictive control for multimode power-split hybrid electric vehicles: Parametric internal model with integrated mode switch and variable meshing losses. Mechanism and Machine Theory, 192: 105543. https://doi.org/10.1016/j.mechmachtheory.2023.105543

[19] Haubensak, L., Strahl, S., Braun, J., Faulwasser, T. (2024). Towards real-time capable optimal control for fuel cell vehicles using hierarchical economic MPC. Applied Energy, 366: 123223. https://doi.org/10.1016/j.apenergy.2024.123223

[20] Betancourt, J., Zhao, C., Tuo, M. (2025). Comparative analysis of EV battery degradation: Real-world data vs. lab simulations. In 2025 IEEE Texas Power and Energy Conference (TPEC), College Station, TX, USA, pp. 1-6. https://doi.org/10.1109/tpec63981.2025.10907087

[21] Wang, D., Zheng, W., Li, S., Chen, Y., Lin, X., Wang, Z. (2025). Impact analysis of uncertainty in thermal resistor-capacitor models on model predictive control performance. Energy and Buildings, 328: 115112. https://doi.org/10.1016/j.enbuild.2024.115112

[22] Zadeh, L.A. (2009). Fuzzy logic. In Encyclopedia of Complexity and Systems Science, Berlin, Germany: Springer, pp. 469-482.

[23] Mendel, J.M. (2024). Type-1 fuzzy sets and fuzzy logic. In Explainable Uncertain Rule-Based Fuzzy Systems, Cham: Springer International Publishing, pp. 17-73. https://doi.org/10.1007/978-3-031-35378-9_2

[24] Pei, P., Meng, Y., Chen, D., Ren, P., Wang, M., Wang, X. (2023). Lifetime prediction method of proton exchange membrane fuel cells based on current degradation law. Energy, 265: 126341. https://doi.org/10.1016/j.energy.2022.126341

[25] Tran, N.S., Lai, K.L., Dao, P.N. (2024). A novel model predictive control for an autonomous four-wheel independent vehicle. International Journal of Mechanical Engineering and Robotics Research, 13: 509-515. https://doi.org/10.18178/ijmerr.13.5.509-515

[26] Masisi, L. (2023). Comparison between a three-level inverter synchronous reluctance machine and a permanent magnet assisted synchronous reluctance machine drives. In 2023 31st Southern African Universities Power Engineering Conference (SAUPEC), Johannesburg, South Africa, pp. 1-6. https://doi.org/10.1109/saupec57889.2023.10057903

[27] Taieb, A., Mukhopadhyay, S., Al-Othman, A. (2022). Adaptive estimation of PEMFC stack model parameters-An experimental verification. International Journal of Hydrogen Energy, 47(98): 41663-41682. https://doi.org/10.1016/j.ijhydene.2022.05.215

[28] Fathabadi, H. (2018). Novel fuel cell/battery/supercapacitor hybrid power source for fuel cell hybrid electric vehicles. Energy, 143: 467-477. https://doi.org/10.1016/j.energy.2017.10.107

[29] Choi, Y., Kim, M., Park, J., Goo, Y. (2025). Proton exchange membrane fuel cell stack durability prediction using arrhenius-based accelerated degradation model. Applied Sciences, 15(3): 1300. https://doi.org/10.3390/app15031300

[30] Setiawan, Y., bin Muhamad Said, M.F., Sutjiadi, A. (2025). Thermal behaviour of electric vehicle battery packs under NEDC and WLTP driving cycles: A GT-

suite simulation study. Cylinder: Jurnal Ilmiah Teknik Mesin, 11(1): 6678. https://doi.org/10.25170/cylinder.v11i1.6678
[31] Jafari, A., Nikoo, M.S., van Erp, R., Matioli, E. (2020). Optimized kilowatt-range boost converter based on impulse rectification with 52 kW/l and 98.6% efficiency. IEEE Transactions on Power Electronics, 36(7): 7389-7394. https://doi.org/10.1109/tpel.2020.3045062
[32] Puranik, I., Zhang, L., Qin, J. (2018). Impact of low-frequency ripple on lifetime of battery in MMC-based battery storage systems. In 2018 IEEE Energy Conversion Congress and Exposition (ECCE), pp. 2748-2752. https://doi.org/10.1109/ecce.2018.8558061
[33] Bambang, R.T., Rohman, A.S., Dronkers, C.J., Ortega, R., Sasongko, A. (2014). Energy management of fuel cell/battery/supercapacitor hybrid power sources using model predictive control. IEEE Transactions on Industrial Informatics, 10(4): 1992-2002. https://doi.org/10.1109/TII.2014.2333873
[34] Feng, J., Han, Z. (2023). Progress in research on equivalent consumption minimization strategy based on different information sources for hybrid vehicles. IEEE Transactions on Transportation Electrification, 10(1): 135-149. https://doi.org/10.1109/TTE.2023.3258639
[35] Ulmer, M.W. (2020). Horizontal combinations of online and offline approximate dynamic programming for stochastic dynamic vehicle routing. Central European Journal of Operations Research, 28(1): 279-308. https://doi.org/10.1007/s10100-018-0588-x

NOMENECLATURE

Abbreviations

AFLC	Adaptive Fuzzy Logic Controller
EMS	Energy Management Strategy
FCEV	Fuel Cell Electric Vehicle
HESS	Hybrid Energy Storage System
PEMFC	Proton Exchange Membrane Fuel Cell
SC	Supercapacitor
SynRM	Synchronous Reluctance Motor
WLTP	Worldwide Harmonized Light Vehicle Test Procedure
SoC	State of Charge
UDDS	Urban Dynamometer Driving Schedule
HWFET	Highway Fuel Economy Test
MPC	Model Predictive Control
RL	Reinforcement Learning
ECMS	Equivalent Consumption Minimization Strategy

Symboles

A_{cell}	Fuel cell active area (cm^2)
C	Supercapacitor capacitance (F)
E_{nernst}	Nernst potential (V)
F	Faraday constant (96485 C/mol)
i_0	Exchange current density (A/cm^2)
K	Power distrubition coefficient
m	Vehicle mass (kg)
N_{cells}	Number of fuel cell stack cells
P	Power (W)
Q	Battery capacity (Ah)
R	Universal gas constant (8.314 J/(mol·K))
T	Temperature (K)
V	Voltage (V)
α	Adaptative coefficient
η	Efficiency
μ	Membership function
τ_{adapt}	Adaptive mechanism time constant (s)